



Coordination Chemistry Reviews

journal homepage: www.elsevier.com/locate/CCR

Review

Strategies towards single-chain magnets

Hao-Ling Sun^{a,b}, Zhe-Ming Wang^a, Song Gao^{a,*}^a Beijing National Laboratory for Molecular Sciences, State Key Laboratory of Rare Earth Materials Chemistry and Applications, College of Chemistry and Molecular Engineering, Peking University, Beijing 100871, PR China^b Department of Chemistry, Beijing Normal University, Beijing 100875, PR China

Contents

1. Introduction	1082
2. Ferromagnetic (<i>F</i> O) strategy towards SCM	1082
2.1. Homospin ferromagnetic SCM	1082
2.2. Heterospin ferromagnetic SCM	1085
2.3. Ferromagnetic SCM based on metal clusters	1087
3. Ferrimagnetic (<i>F</i> I) strategy towards SCM	1090
3.1. Organic radical-bridged ferrimagnetic SCM	1090
3.2. Oxamate-bridged ferrimagnetic SCM	1091
3.3. Cyanide-bridged ferrimagnetic SCM	1092
3.4. Other ligand-bridged ferrimagnetic SCM	1092
3.5. Homospin ferrimagnetic SCM	1092
4. Weak ferromagnetic (<i>WF</i>) strategy towards SCM	1094
4.1. Phosphate-bridged weak ferromagnetic SCM	1094
4.2. Organic radical-bridged weak ferromagnetic SCM	1094
4.3. <i>EE</i> -azido-bridged weak ferromagnetic Ni ²⁺ chain	1095
4.4. Phosphinate-bridged weak ferromagnetic SCM	1096
4.5. Tetrazolate-bridged weak ferromagnetic SCM	1096
4.6. Weak ferromagnetic SCM based on [Mn ₃ O] unit	1097
5. Conclusion and perspective	1099
Acknowledgements	1099
References	1100

ARTICLE INFO

Article history:

Received 21 October 2009

Accepted 9 February 2010

Available online 16 February 2010

Keywords:

Single-chain magnets

Magnetic structure

Synthesis strategy

ABSTRACT

Single-chain magnets (SCM) are a novel class of molecular magnetic materials exhibiting slow magnetic relaxation, which arises from large uniaxial type magnetic anisotropy, strong intrachain and very weak or negligible interchain magnetic interactions. Although more than 20 examples of SCM have been reported, the controlled synthesis of SCM is still a challenge. Here we review the three strategies for the construction of SCM, highlight typical examples, discuss the role of intrachain and interchain interactions on the overall magnetic behavior of SCM as well as how to control or tune these interactions. For each strategy we present the advantages/shortcoming and then point out the main directions that remain to be developed in the field.

© 2010 Elsevier B.V. All rights reserved.

Abbreviations: SCM, single-chain magnets; *F*O, ferromagnetic; *Fl*, ferrimagnetic; *AF*, antiferromagnetic; *WF*, weak ferromagnetic; *FCM*, field-cooled magnetization; *ZFCM*, zero-field-cooled magnetization; LRO, long range ordering; NMR, ¹H nuclear magnetic resonance; μSR, muon spin rotation; 1D, one-dimensional; 2D, two-dimensional; 3D, three-dimensional; NN, nearest-neighbor; NNN, next-nearest-neighbor; *EO*, end-on; *EE*, end-to-end; *bt*, 2,2'-bithiazol; bpeado, 1,2-bis(4-pyridyl)-ethane-N,N'-dioxide; trans-1,2-chdc, trans-1,2-cyclohexanedicarboxylate; bispicen, N,N-bis(2-pyridylmethyl)-1,2-ethanediamine; Cl₄Cat, tetrachlorocatecholate dianion; bpy, 2,2'-bipyridine; phen, 1,10-phenanthroline; bpym, 2,2'-bipyrimidine; Tp, tris(pyrazolyl)hydriborate; ox, oxalate; 5-MeOsalen, N,N'-ethylenebis(5-methoxysalicylideneiminate); Hacac, acetylacetone; 5,5'-Me₂salen, N,N'-bis(5,5'-dimethylsalicylidene)-o-ethylenediamine; pao, pyridine-2-aldoximate; saltmen, N,N'-(1,1,2,2-tetramethylethylene)bis(salicylideneiminate); py, pyridine; dpkd, dpkme, the diolate derivative of di-2-pyridylketone; hfac, hexafluoroacetylacetone; NITPhOMe, 4-methoxy-phenyl-4,4,5,5-tetramethylimidazoline-1-oxyl-3-oxide; BPNN, p-butoxyphenyl-nitronyl nitroxide; 5-TMAMsaltmen, N,N'-(1,1,2,2-tetramethylethylene)bis(5-trimethylammoniomethyl-salicylideneiminate); TCNQ, tetra-p-quinodimethane; 2,4,6-tmpa, N-2,4,6-trimethylphenyloxamate; bpca, bis(2-pyridylcarbonyl)amine; bime, 1,2-bis(imidazol-1'-yl)ethane; HO-BDC, 5-hydroxyisophthalic acid; NITEE, 4-ethyl-4,4,5,5-tetramethylimidazoline-1-oxyl-3-oxide; NITPhOPh, 4-phenoxy-benzyl-4,4,5,5-tetramethylimidazoline-1-oxyl-3-oxide; bmdt, N,N'-bis(4-methoxylbenzyl)-diethylenetriamine; TPP, meso-tetraphenylporphyrin; cyclam, 1,4,8,11-tetraazacyclotetradecane; H₂bdt, 5,5'-(1,4-phenylene)bis(1H-tetrazole); tBusao, 3,5-di-tert-butylsalicylaldoxime.

* Corresponding author. Tel.: +86 10 62767569; fax: +86 10 62751708.

E-mail address: gaosong@pku.edu.cn (S. Gao).

Three Strategies towards Sing-Chain Magnets:



Scheme 1. Three strategies towards single-chain magnets.

1. Introduction

The last 10 years witnessed the growth and success in the research field of single-chain magnets (SCM) [1–23]. As an analogue to single-molecular magnets (SMM), SCM also show the unique feature of slow magnetic relaxation and magnetic hysteresis of molecular origin [24]. The original motivation for constructing SCM is to increase the blocking temperature of SMM so as to fulfill the condition for their future application as molecular memory devices or recording media. The first prediction for SCM was made by Glauber in 1963 [25]; however, the first SCM example was reported by Gatteschi et al. in 2001, 38 years after the Glauber's prediction [12]. According to Glauber's theory, the origin of the slow magnetic relaxation was tracked to the large uniaxial type magnetic anisotropy, strong intrachain magnetic interaction, and negligible interchain interactions that hamper the transition to 3D magnetic ordering. Therefore, the synthetic approaches to build SCM include two respects: (i) to utilize appropriate bridging ligands as effective magnetic couplers to link uniaxial, anisotropic spin carriers, such as Co^{2+} , Ni^{2+} , Mn^{3+} , Fe^{2+} and lanthanide ions, into 1D chains and (ii) to use suitable diamagnetic separators so as to make these chains magnetically well isolated [2–23]. In SCM literature, oxygen [8,9,11], cyano [5,6,8,9,15], oximate [10], azido [2,11,20], oxalato/oxamate [7,14], carboxylate [3,17], phosphate/phosphinate [18,21] and organic radical [12,13,19] have been employed as bridging ligands because they can transport magnetic coupling efficiently. On the other hand, bulk co-ligands, long spacers, counter ions, etc., have been used for the purpose to reduce interchain interactions, and some co-ligands themselves also serve as intrachain bridges. The various combinations of intra-chain bridges, metal ions, and separators have led to many SCMs with different spin structures (**Scheme 1**).

From the point view of magnetism, in the field of molecular magnetism there are three possible approaches for the construction of 3D ordered magnets with spontaneous magnetization. These are ferromagnetic (FO), ferrimagnetic (FI) and weak ferromagnetic (WF) approaches [26]. Compared with ferrimagnets and weak ferromagnets, ferromagnets are relatively rare due to the fact that FO interactions relying on the orthogonality of the magnetic orbitals of the interacting spin carriers are significantly weaker and less com-

mon than AF ones [26]. These approaches also work in SCM area. This article will focus on the demonstration of the three strategies in the construction of SCM, the key examples (from homospin systems to heterospin systems to systems based on metal clusters), experimentally characterization and rationalization of this novel class of molecular magnets. The role of bridging ligands, the influence of interchain magnetic coupling on the final magnetic behavior and the ways for weakening the interchain interaction will be briefly discussed. Finally, we summarize the novelty/shortcoming of these strategies and highlight our current understanding and future development of this field.

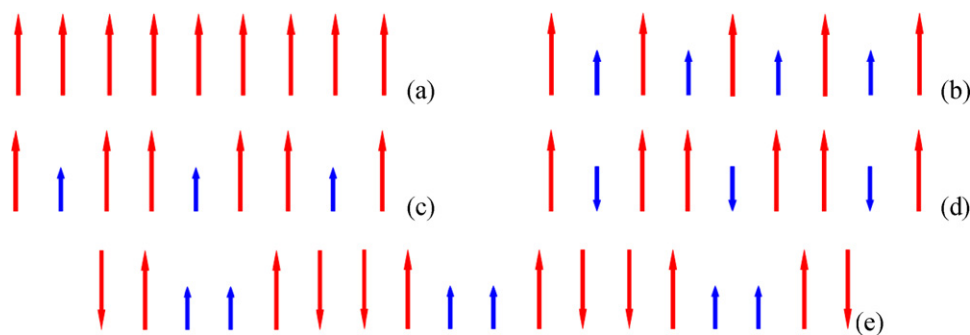
2. Ferromagnetic (FO) strategy towards SCM

When we try to design and synthesize magnetic materials, the first choice is usually to align spins in a parallel fashion because this alignment will give the largest spin ground state, which might result in novel materials. However, a parallel spin arrangement is relatively rare due to the large dipole–dipole energy. In the SCM field, the FO strategy is first considered because the larger the spin ground state of the system, the higher will be the blocking temperature. One way to get FO SCM is to make use Kahn's theory to arrange the magnetic orbitals of the spin carriers orthogonally so as to favor ferromagnetic interaction [26]. Another way is to make use the reported FO pathways in the field of molecular magnetism, such as end-on (EO)–azido [2,11] or phenolate oxygen in Mn^{3+} –Schiff base dimers [8–10]. Up till now, there have been about ten examples of SCM with different spin structures (**Scheme 2**), in which anisotropic spin carriers (including homospin, heterospin and metal cluster) are ferromagnetically coupled. These examples will be described in detail in the following sections.

2.1. Homospin ferromagnetic SCM

Although Glauber suggested that ferromagnetically coupled spin carriers with strong anisotropy would show slow relaxation of magnetization in 1963, the first real homospin FO SCM, $\text{Co}(\text{bt})(\text{N}_3)_2$ (**1**), was reported in 2003 by our group [2a]. In this compound, Co^{2+} metal ions are bridged by double EO-azido ligands, forming a 1D structure in which there are three independent octahedral Co sites, leading to a helical arrangement of the Co^{2+} metal ions along the chain (**Fig. 1a**). In an octahedral coordination environment, Co^{2+} metal ions can be considered as an effective $S = 1/2$ spin with highly anisotropic g values at low temperature. As expected, the EO-azido bridges transmit strong ferromagnetic intrachain interactions between Co^{2+} ions [27] and the chelating bulky bt ligands magnetically isolate these chains. This fulfills the condition suggested by Glauber for SCM exhibiting slow magnetic relaxation.

Dc magnetic susceptibility above 100 K was fitted according to a Heisenberg $S = 3/2$ chain ($H = -2J\sum_i \text{S}_i \cdot \text{S}_{i+1}$) model [28]. The intrachain interactions between Co^{2+} were FO with $J = +6.2 \text{ cm}^{-1}$ (**Fig. 1b**).



Scheme 2. Spin structures found in reported ferromagnetic SCM.

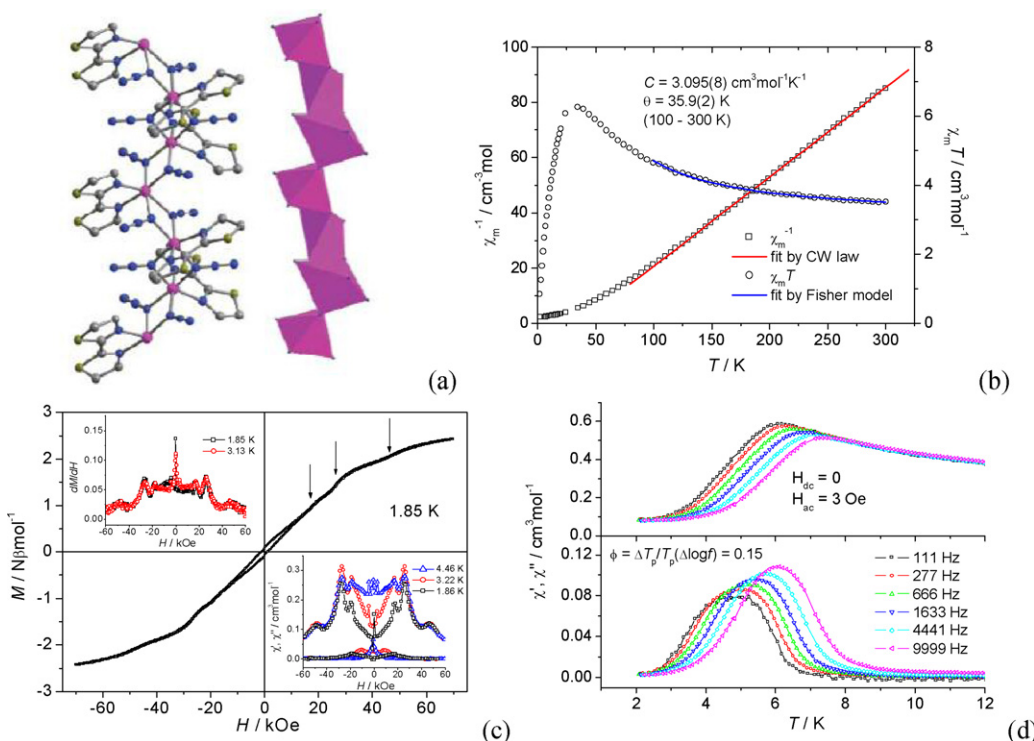


Fig. 1. (a) The 1D helical cobalt-azido chain in **1**; (b) $\chi_m T$ - T plots and the fitting of magnetic data by fisher model; (c) field dependence of magnetization measured at 1.85 K. (Inset) Upper left, field dependence of dM/dH ; lower right, field dependence of *ac* susceptibility. (d) Temperature dependence of χ'_M and χ''_M of the *ac* susceptibility in zero applied static field. Copyright 2003 American Chemical Society.

Above 6 K, the exponential increase of the $\ln(\chi_M T)$ vs. $1/T$ plot further confirms the 1D nature of the system and its Ising-like magnetic anisotropy. Slow relaxation of the magnetization is observed on the field dependence of the magnetization at 1.85 K, which exhibits a hysteresis effect with a coercive field of about 1000 Oe. Moreover, step features are observed at 17, 26 and 46 kOe, which are attributed to the presence of different anisotropy axes of Co^{2+} in the helical chain (Fig. 1c). The relaxation time of the system was studied using *ac* susceptibility measurements above 1.8 K. As shown in Fig. 1d, strong frequency dependence of χ'_M and χ''_M of *ac* susceptibility is observed. The relaxation time deduced from the *ac* data follows an Arrhenius law with $\tau_0 = 3.4 \times 10^{-12} \text{ s}$ and $\Delta E/k_B = 94(2) \text{ K}$. The relaxation mode was broad and was fitted with a generalized Debye model [29], taking into account a distribution of relaxation quantified by the parameter of α values between 0.65 and 0.7. In addition, the second harmonics are negligibly small, essentially at a noise level, which excludes any spontaneous moment and supports the low dimensionality of this compound. The heat-capacity measurements do not show any λ peak down to 1.8 K, which also support the SCM behavior of this compound [26].

Enlightened by the successful preparation of $\text{Co}(\text{bt})(\text{N}_3)_2$ SCM, we are confident that the EO-azido bridged Co^{2+} chains should be SCM, provided interchain interaction is small. Thus, in the next step we attempt to prepare isolated 1D Co^{2+} chains by using a long spacer co-ligand of bpeado [2b]. This strategy proved to be successful and a 1D compound with the formula $[\text{Co}(\text{N}_3)_2(\text{H}_2\text{O})_2]\cdot(\text{bpeado})$ (**2**) was created where the 1D Co^{2+} -azido chains are isolated by bpeado (Fig. 2a and b). Compared with the previous $\text{Co}(\text{bt})(\text{N}_3)_2$ SCM, the connection between the Co^{2+} ions is the same; however, the chain structure is quite different. This compound has only one unique Co^{2+} center and the remarkable feature is the perfectly straight alignment of metal ions within the chain. This alignment makes the easy axis of all Co^{2+} ions point to one direction without reducing the magnetic anisotropy, probably resulting in a strong-

magnetically anisotropic Ising chain. The bpeado does not act as a ligand, but hydrogen-bonds to coordinated water and also separates the chains.

The *dc* magnetic studies on powder sample revealed strong intrachain and weak interchain ferromagnetic coupling ($J = 10.0 \text{ cm}^{-1}$, $zJ = 0.3 \text{ cm}^{-1}$), indicative of the 1D magnetic nature in this compound. Interestingly, the *ac* signal of χ'_M and χ''_M show two frequency-dependent peaks, indicating two magnetic transitions. Further magnetic studies proved that the magnetic transition at higher temperature is 3D LRO together with spin-glass behavior (due to the relatively strong ferromagnetic interchain interaction in a dipole manner), while, the lower temperature one is a characteristic superparamagnetic behavior of SCM with the energy barrier and the relaxation time of 56 K and $2.5 \times 10^{-9} \text{ s}$, respectively (Fig. 2c). In addition, a magnetic study was also performed using large single crystals. The ZFCM and FCM plots under 10 Oe and along different crystal axis are similar in shape, but the magnetization along *a*-axis is about 100 times larger than the ones along the other two axes, indicating strong Ising type magnetic anisotropy in this compound (Fig. 2d).

In the two examples above, EO-azido is used as ferromagnetic interaction coupler to construct SCM due to its contribution to *FO* coupling. Besides azido, other ligands such as carboxylate can also transmit *FO* coupling and so they can also be used for the construction of SCM. In 2006, Chen et al. reported a layer compound $\text{Co}(\text{trans}-1,2-\text{chdc})$ (**3**) that exhibits slow magnetic relaxation [3a]. In this compound, carboxylate bridges Co^{2+} to form a paddle-wheel chain and the chains are further connected by cyclohexane groups, resulting in a 2D layer structure (Fig. 3a). From a magnetic point of view, the layer compound can be described as a magnetic chain compound because the magnetic interaction transmitted by carboxylate within the paddle-wheel chain is much stronger than that between the chains, the diamagnetic cyclohexane groups act as spacers to make these chains magnetically isolated.

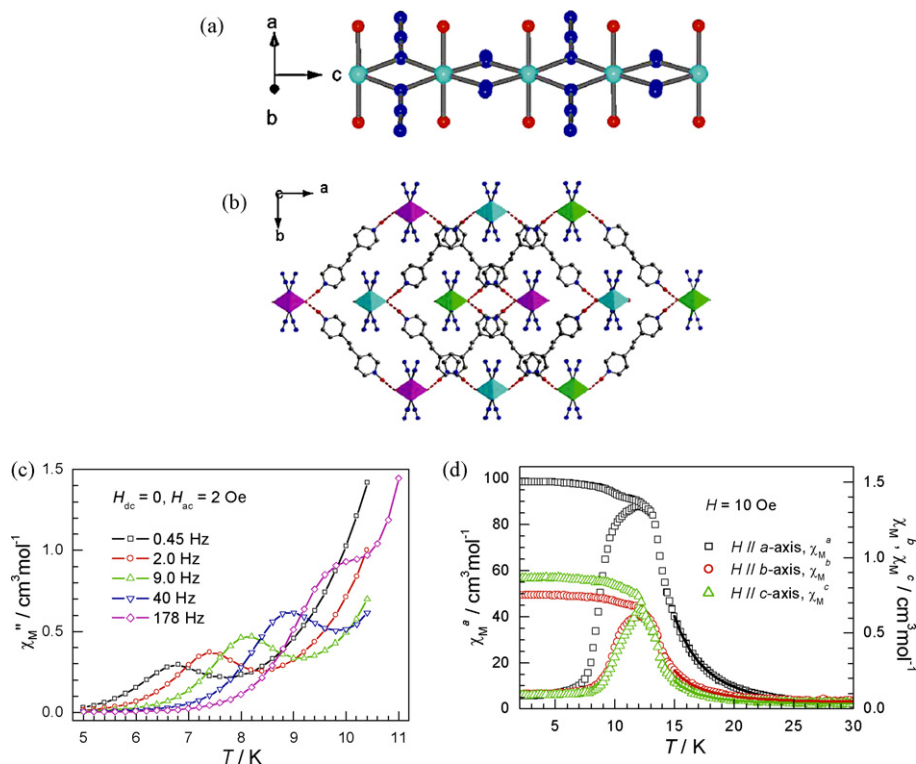


Fig. 2. The 1D cobalt-azido chain in **2**; (b) the interchain relationship with bpeado hydrogen-bonding to the coordinated water of Co^{2+} and isolating the chains; (c) frequency dependence of χ_M'' of the ac susceptibility at low-temperature region; (d) the ZFCM/FCM curves under 10 Oe along three different crystallographic axes, showing the Ising type anisotropy.

Dc susceptibility studies at high temperature were performed and a preliminary analysis of the data by using 1D alternating chain model led to an estimation of the ferromagnetic coupling ($J/k_B = 11.51 \text{ K}$ and 3.95 K) between Co^{2+} (Fig. 3b). Further dc magnetic measurements of single crystal samples revealed

the uniaxial anisotropy. $\text{Co}(\text{trans}-1,2\text{-chdc})$ exhibits χ'_M and χ''_M ac susceptibility signals at low temperature which are frequency dependent (Fig. 3c and d). The fitting of the ac data by using Arrhenius law gave two physical relaxation time scales, $\tau_1 = 5.19 \times 10^{-11} \text{ s}$ and $\tau_2 = 5.59 \times 10^{-8} \text{ s}$ for the high- and

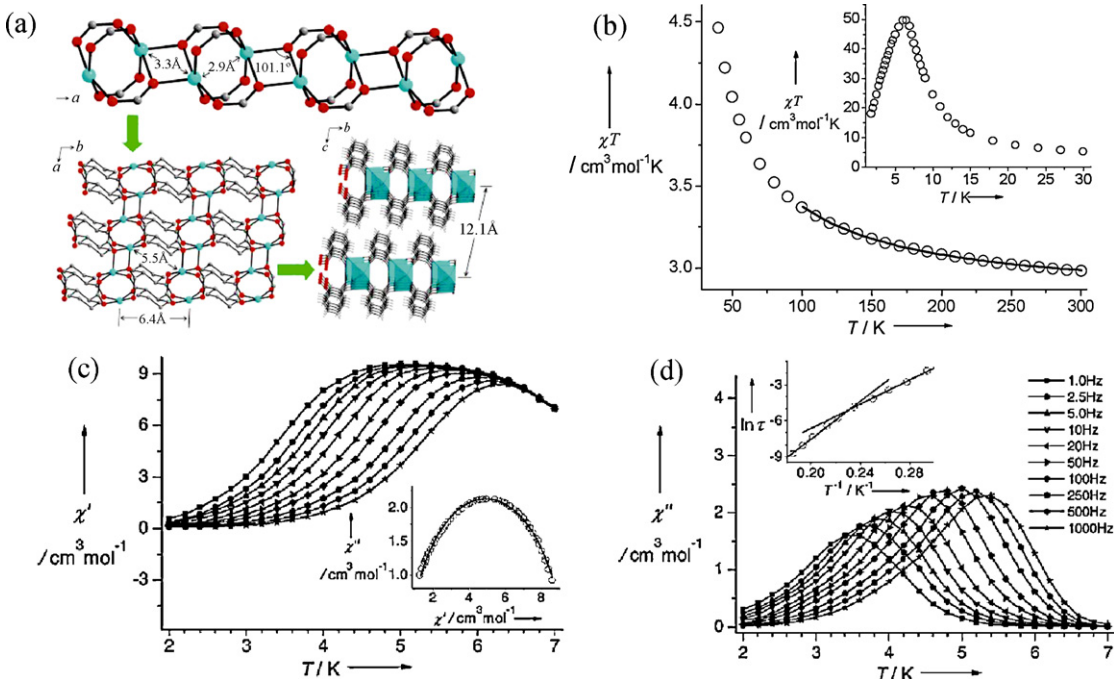


Fig. 3. (a) Perspective views of the paddle-wheel chain, layer, and crystal packing in **3**; (b) $\chi_M T$ - T plots from 50 to 300 K; solid line: fitted by the modified Fisher model for 1D alternating chain. Inset: $\chi_M T$ vs. T plot from 2 to 30 K. (c) χ'_M of ac susceptibility (inset: Cole-Cole diagram at 4.2 K); (d) χ''_M of ac susceptibility (inset: peak temperatures of χ''_M fitted by Arrhenius law); reprinted with permission from Ref. [3a]. Copyright 2006 Wiley.

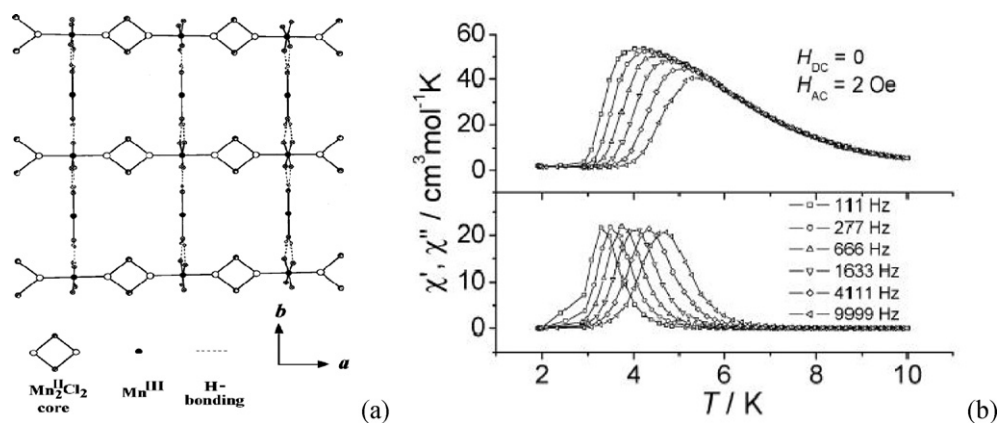


Fig. 4. (a) Skeletal representation of **4** in the *ab* plane; (b) χ'_M and χ''_M of the *ac* susceptibility in zero applied static field. Copyright 2004 American Chemical Society.

low-temperature regions, respectively; and two corresponding different barriers $\Delta\tau_1/k_B = 80.9$ and $\Delta\tau_2/k_B = 50.2$ K. This result is in agreement with the observed finite-size effect halving the Glauber activation barrier for SCM [30]. A Cole–Cole plot at 4.2 K has been fitted to a generalized Debye model with an α value of 0.10 indicating a narrow distribution of relaxation time [29].

Besides covalent bonds, weak interactions such as hydrogen bonding can also transmit FO coupling. One example of hydrogen-bonded 1D arrangement showing slow magnetic relaxation has been reported by Banerjee and Gao et al. [4]. The compound of formula $\text{Mn}^{2+}_2(\text{bispicen})_2(\mu_3\text{-Cl}_2)_2\text{Mn}^{3+}(\text{Cl}_4\text{Cat})_2\text{Mn}^{3+}(\text{Cl}_4\text{Cat})_2(\text{H}_2\text{O})_2$ (**4**) has a 2D network structure, in which the $\mu_3\text{-Cl}^-$ ions connect Mn^{2+} and Mn^{3+} to form 1D chains along *a*-axis and these chains are further connected by hydrogen bonding between the coordinated water molecules and Cl_4Cat (Fig. 4a). Because of Cl-bridged Mn^{2+} dimer and the strong intradimer AF interaction, the compound has been described as a chain of ferromagnetically coupled Mn^{3+} .

Dc magnetic susceptibility indicates ferromagnetic interaction [of about $+0.96(8)\text{ cm}^{-1}$] between Mn^{3+} mediated through strong hydrogen bonds. The magnetic dynamics investigated by *ac* susceptibility measurement indicates slow magnetic relaxation of typical SCM with narrow distribution of relaxation time (Table 1).

2.2. Heterospin ferromagnetic SCM

In addition to homospin FO chains, there are heterospin ferromagnetic chains, in which more than one kind of spin carriers is aligned in parallel. In the field of molecular magnetism, metal cyanide units, such as $\text{Fe}(\text{CN})_6^{3-}$, $\text{Cr}(\text{CN})_6^{3-}$, $\text{Mn}(\text{CN})_6^{3-}$ and their derivatives have proven to be suitable building blocks for the construction of heterospin FO materials. For this reason, when one tries to synthesize heterospin FO SCMs, these cyanide building blocks are naturally chosen [26a]. Thus several heterospin FO SCMs have been obtained by using versatile metal cyanide building blocks such as $\text{Fe}(\text{L}1)(\text{CN})_4^-$ and $\text{Fe}(\text{L}2)(\text{CN})_3^-$ (where L1 is bpy or phen or bpym and L2 is Tp) together with Co^{2+} or Cu^{2+} metal ions [5,6]. These chains are made of corner-shared Fe_2M_2 squares, in which the metal ions are connected by double metal cyanide units (Fig. 5a). Two typical examples are $[\text{Fe}(\text{bpy})(\text{CN})_4]_2\text{Co}(\text{H}_2\text{O})_2\cdot 4\text{H}_2\text{O}$ (**5**) and $[\text{Fe}(\text{Tp})(\text{CN})_3]_2\text{Cu}(\text{CH}_3\text{OH})\cdot 2\text{CH}_3\text{OH}$ (**6**), and the intrachain $\text{Fe}^{3+}\cdots\text{M}^{2+}$ ($\text{M}=\text{Co}$ or Cu) coupling is FO based on *dc* magnetic susceptibility measurements, data analysis and DFT calculations [5].

For **5**, the FCM measurements on single crystals along different crystal axes indicate Ising type magnetic anisotropy in this compound (Fig. 5b). The strong dependence of coercive field on the temperature and the sweep rate and/or the frequency-dependent *ac* signal in a zero *dc* magnetic field demonstrates the existence of slow magnetic relaxation (Fig. 5c). The relaxation

Table 1

Summary of the fitting results of the *ac* magnetic data by using the Arrhenius law or generalized Debye model.

Comp.	$\Delta E_1/k_B$ [K]	τ_{01} [s]	$\Delta E_2/k_B$ [K]	τ_{02} [s]	α	Ref.
1	94(2)	3.4×10^{-12}	–	–	0.65–0.7	[2a]
2	56	2.5×10^{-9}	–	–	–	[2b]
3	80.9	5.19×10^{-11}	50.2	5.59×10^{-8}	0.10	[3a]
4	50.5(5)	3.4×10^{-10}	–	–	0.3	[4]
5	142	9.4×10^{-12}	–	–	–	[5b]
6	112.3	2.8×10^{-13}	–	–	0.52	[6]
7	46.9	4.4×10^{-10}	–	–	0.3	[7]
8	31	3.7×10^{-10}	25	3×10^{-8}	0.06	[8]
9	16.4	3.04×10^{-7}	–	–	–	[9]
10a	72(1)	$5.5(1) \times 10^{-11}$	–	–	–	[10a]
11	42	3.5×10^{-11}	–	–	0.35	[11]
12	153 (2)	$3.0(2) \times 10^{-11}$	–	–	–	[12]
13	91.4	2.1×10^{-10}	67.7	6.8×10^{-6}	0.10	[13]
14	23.5	4.0×10^{-9}	–	–	0.05	[14]
15	25.8	3.9×10^{-10}	–	–	0.057	[15]
16	27(1)	$1.6(6) \times 10^{-8}$	–	–	0.09–0.13	[16]
17	76(1)	1.1×10^{-9}	–	–	0.50	[17]
18	45.2	1.13×10^{-13}	–	–	0.15–0.35	[18]
19	69	1.9×10^{-12}	42	5.6×10^{-10}	0.16	[19a]
21	36.8(6)	$1.6(4) \times 10^{-10}$	–	–	0.014–0.076	[21]
22	43.5	5.1×10^{-9}	–	–	0.1	[22]
23b	96.6	3.7×10^{-11}	–	–	0.17	[23b]

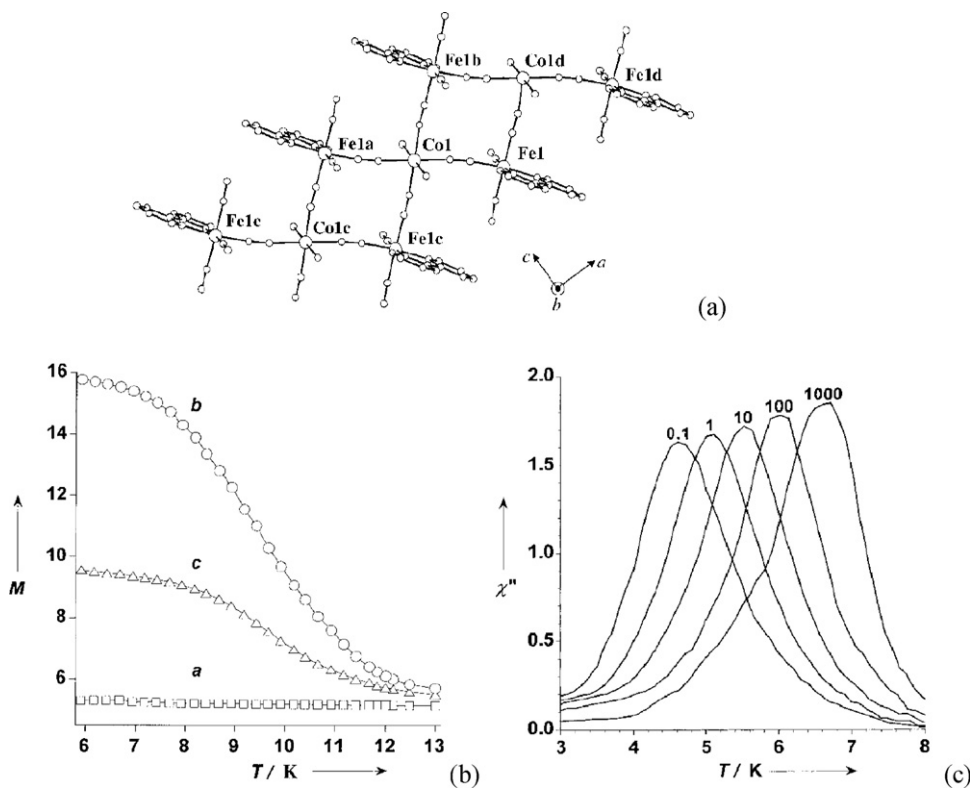


Fig. 5. (a) Perspective view of a fragment of the double zigzag chain of **5** running parallel to the *a*-axis; (b) FCM of a single crystal along the *a*, *b*, and *c* axes; (c) temperature dependence of χ''_M of the *ac* susceptibility on a single crystal in zero applied static field; reprinted with permission from Ref. [5b]. Copyright 2003 Wiley.

time extracted from *ac* data follows an activated behavior with $\tau_0 = 9.4 \times 10^{-12}$ s and $\Delta E/k_B = 142$ K. The absence of a transition signature in heat-capacity measurements and the presence of slow relaxation support this compound as SCM [5]. **6** shows similar slow magnetic relaxation with an $\Delta E/k_B = 112.3$ K and $\tau_0 = 2.8 \times 10^{-13}$ s (Fig. 6 and Table 1) [6].

An interesting question concerning interchain magnetic interaction arises after the report of another *FO* $\text{Fe}^{3+}-\text{Co}^{2+}$ chain $[\text{Fe}(\text{bpy})(\text{CN})_4]_2\text{Co}(\text{H}_2\text{O})\text{-MeCN}\text{-}0.5\text{H}_2\text{O}$ [31]. The comparison of its magnetic behavior with compound **5** gives us an opportunity to discuss the role of interchain interaction on the overall magnetic behavior. In $[\text{Fe}(\text{bpy})(\text{CN})_4]_2\text{Co}(\text{H}_2\text{O})\text{-MeCN}\text{-}0.5\text{H}_2\text{O}$, the intrachain interaction is *FO*, which is similar to compound **5**; however, the interchain coupling is *AF* with a small value of -0.06 cm^{-1} , resulting in the metamagnetic behavior. However, when the applied *dc* field is larger than the critical field of 600 Oe, frequency dependence in *ac* data appears. This clearly indicates that interchain interaction is another important role governing the overall magnetic behavior. However, until now, although there are some strategies to reduce interchain interaction, the exact control is still a challenge and this requires further investigation.

Another type of building block for constructing heterospin chain is metal oxalate, such as $\text{Fe}(\text{ox})_3^{3-}$, $\text{Cr}(\text{ox})_3^{3-}$ and their derivatives. In 2008, Coronado et al. reported the first oxalate-bridged *FO* heterospin SCM $[\text{K-(18-crown-6)}]_{1/2}[(18\text{-crown-6})(\text{FC}_6\text{H}_4\text{NH}_3)]_{1/2} [\text{Co}(\text{H}_2\text{O})_2\text{Cr}(\text{ox})_3]$ (**7**) [7]. In **7**, $[\text{Cr}(\text{ox})_3]^{3-}$ and $\text{Co}(\text{H}_2\text{O})_2^{2+}$ are connected by the oxalate linkers to form anionic chains with the formula $[\text{Co}(\text{H}_2\text{O})_2\text{Cr}(\text{C}_2\text{O}_4)_3]^-$. These chains are separated by hydrogen bonds between the coordinated water molecules of Co^{2+} ions and the terminal oxalate of Cr^{3+} ions and the diamagnetic cationic layer of $[\text{K-(18-crown-6)}]^+$ and $[(\text{FC}_6\text{H}_4\text{NH}_3)\text{-(18-crown-6)}]^+$ (Fig. 7a and b). The static magnetic measurement indicates *FO* interaction between Co^{2+} and Cr^{3+} transported by bis-bidentate oxalate ligands (Fig. 7c). A hysteresis loop is observed at 2 K ($H_c = 80$ Oe), confirming the magnet-like behavior. However, the heat-capacity measurement down to 2 K does not show any λ peak, excluding the existence of 3D LRO. Further *ac* susceptibility data show strong frequency dependence for both χ'_M and χ''_M signals with the qualified ϕ value of 0.11, indicating superparamagnetic behavior [32]. The fitting of the *ac* susceptibility by using the Arrhenius law and a generalized Debye model suggests the typical magnetic relaxation of SCM with nearly one single process (Table 1).

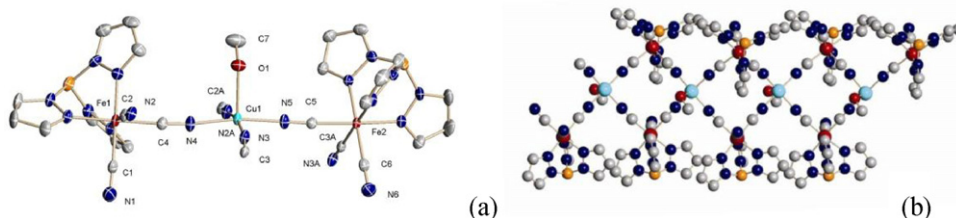


Fig. 6. Structure of segments (a) and the 1D chain (b) of **6**; reprinted with permission from Ref. [6a]. Copyright 2004 American Chemical Society.

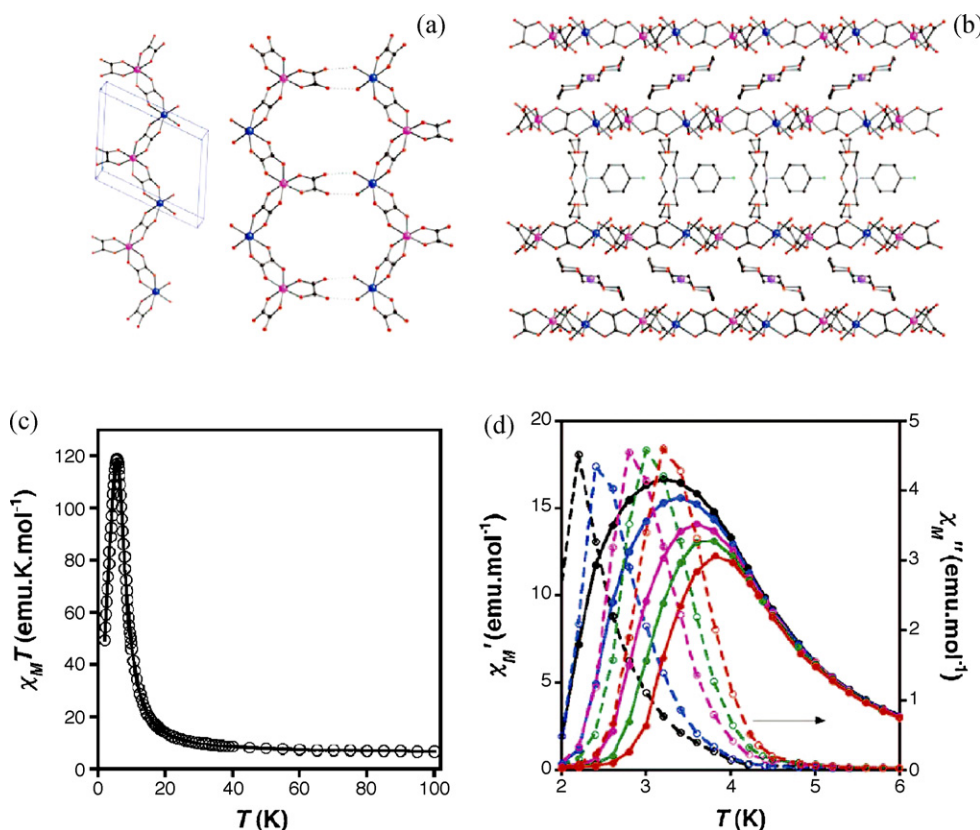


Fig. 7. 1D chain structure (a) and the packing (b) between the chains in **7**; (c) temperature dependence of $\chi_M T$ in the low-temperature regime; (d) χ_M' and χ_M'' dynamic susceptibility; reprinted with permission from Ref. [7]. Copyright 2008 American Chemical Society.

2.3. Ferromagnetic SCM based on metal clusters

In 2005, Miyasaka et al. reported a novel SCM, $(\text{NEt}_4)[\text{Mn}_2(5\text{-MeOsalen})_2\text{Fe}(\text{CN})_6]$ (**8**), which can be considered as 1D *FO* chain constructed by ferromagnetically coupled $[\text{Mn}-\text{NC}-\text{Fe}-\text{CN}-\text{Mn}]$ trinuclear units [8]. Within the trinuclear unit, two $[\text{Mn}(5\text{-MeOsalen})]^+$ are joined with one $[\text{Fe}(\text{CN})_6]^{3-}$ to form a cyano-bridged linear trinuclear $[\text{Mn}-\text{NC}-\text{Fe}-\text{CN}-\text{Mn}]^-$ anion. These trinuclear units are further connected by phenolate oxygen of the Schiff base, forming a 1D anionic linear chain structure with the easy axis of magnetization along the chain direction (Fig. 8a). The $[\text{NEt}_4]^+$ counter ions lie between the chains and make the chains magnetically well separated. The magnetic susceptibility above 10 K was fitted to a Heisenberg model considering the 1D arrangement of $[\text{Mn}^{3+}\dots\text{Fe}^{3+}\dots\text{Mn}^{3+}]$ trimers with $\text{Fe}^{3+}\dots\text{Mn}^{3+}$ *FO* interaction ($J/k_B = +6.5$ K), and the trimers were connected through weak *FO* interactions (treated by mean-field approximation, $zJ'/k_B = +0.07$ K) (Fig. 8b) [33]. The magnetic measurements on single crystal reveal that the easy axis is along the chain direction and the chain is Ising type, and the coercive field along the easy axis shows strong dependence on the temperature and the sweep rate. In addition, the *ac* signals in a zero *dc* magnetic field between 1.82 and 2.9 K show obvious frequency dependence (Fig. 8c). The above magnetic studies demonstrate the existence of slow magnetic relaxation. Further *ac* data measured between 1.82 and 2.9 K show semicircle Cole–Cole curves, indicating a very narrow distribution of relaxation times (Table 1). By combining the *dc* and *ac* data, two relaxation times ($\tau_1 = 3.7 \times 10^{-10}$ and $\tau_2 = 3 \times 10^{-8}$ s) together with two different energy barriers ($\Delta\tau_1/k_B = 31$ and $\Delta\tau_2/k_B = 25$ K) are deduced by using Arrhenius law, which is due to the finite-size effect halving the Glauber activation barrier for SCM [30].

Recently, another *FO* SCM based on ferromagnetically coupled metal clusters, $\{[\text{Mn}(5,5'\text{-Me}_2\text{salen})]\}_2[\text{Ru}(\text{acac})_2(\text{CN})_2]\cdot[\text{Ru}(\text{acac})_2(\text{CN})_2]\cdot 2\text{CH}_3\text{OH}$ (**9**), was reported by Lau and Gao et al. [9]. **9** can also be considered as a 1D *FO* chain constructed by ferromagnetically coupled $[\text{Mn}-\text{NC}-\text{Ru}-\text{CN}-\text{Mn}]$ trinuclear units with a central $[\text{Ru}(\text{acac})_2(\text{CN})_2]^-$ moiety instead of $[\text{Fe}(\text{CN})_6]^{3-}$, compared to Miyasaka's SCM. The trinuclear units are further linked together by intermolecular face-to-face $\pi-\pi$ interactions between neighboring (5,5'-Me₂salen) ligands and weak $\text{Mn}\cdots\text{O}^*$ (phenolate oxygen of the adjacent trinuclear unit) interactions, resulting in a 1D linear chain structure (Fig. 9a). The free $[\text{Ru}(\text{acac})_2(\text{CN})_2]^-$ anions and the methanol molecules are situated between the polymeric chains, separating the chains well (Fig. 9b). The *dc* magnetization study indicates totally *FO* coupling within the chain. Based on the structure feature, two different exchange couplings can be identified along the chain: (i) J_1 the $\text{Mn}^{3+}\cdots\text{Ru}^{3+}$ interaction via a cyano bridge and (ii) J_2 the $\text{Mn}^{3+}\cdots\text{Mn}^{3+}$ exchange via phenolate oxygen bridges. The best fitting of magnetic data in the range of 3–300 K by using a Heisenberg trinuclear model ($S_{\text{Mn}}, S_{\text{Ru}}, S_{\text{Mn}} = 2, 1/2, 2$) with the consideration of inter trinuclear and interchain magnetic coupling gives the following result with the parameters $J_1 = +0.87 \text{ cm}^{-1}$, $J_2 = +0.24 \text{ cm}^{-1}$ and $zJ' = +0.004 \text{ cm}^{-1}$ (Fig. 9c). All these observations indicate that this chain compound should be a SCM because the anisotropic Mn^{3+} , the strong intrachain and very weak interchain interaction found in this compound fulfill the conditions required by SCM. Further *ac* susceptibility measurements show obvious frequency dependence both in the χ_M' and χ_M'' signals and the relaxation time of 3.04×10^{-7} s and energy barrier of 16.4 K can be deduced from the Arrhenius law, indicating the superparamagnetic behavior of SCM (Fig. 9d).

Besides the *FO* chains based on ferromagnetically coupled metal clusters, there is another type of *FO* chain constructed by

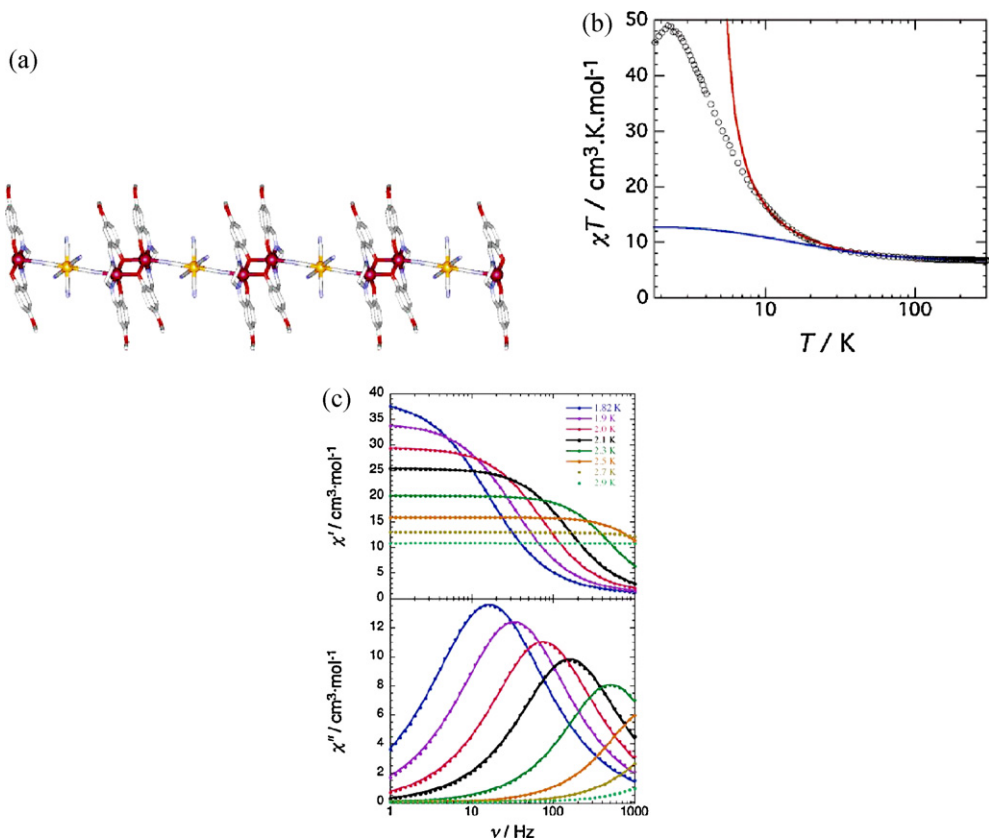


Fig. 8. (a) 1D assembly of Mn³⁺-Fe³⁺-Mn³⁺ trinuclear units in **8**; (b) χ_T - T plots and the fitting of magnetic data by a trimer model; (c) frequency dependence of the ac susceptibility. The solid lines are the best fits obtained with the generalized Debye model; reprinted with permission from Ref. [8]. Copyright 2005 American Chemical Society.

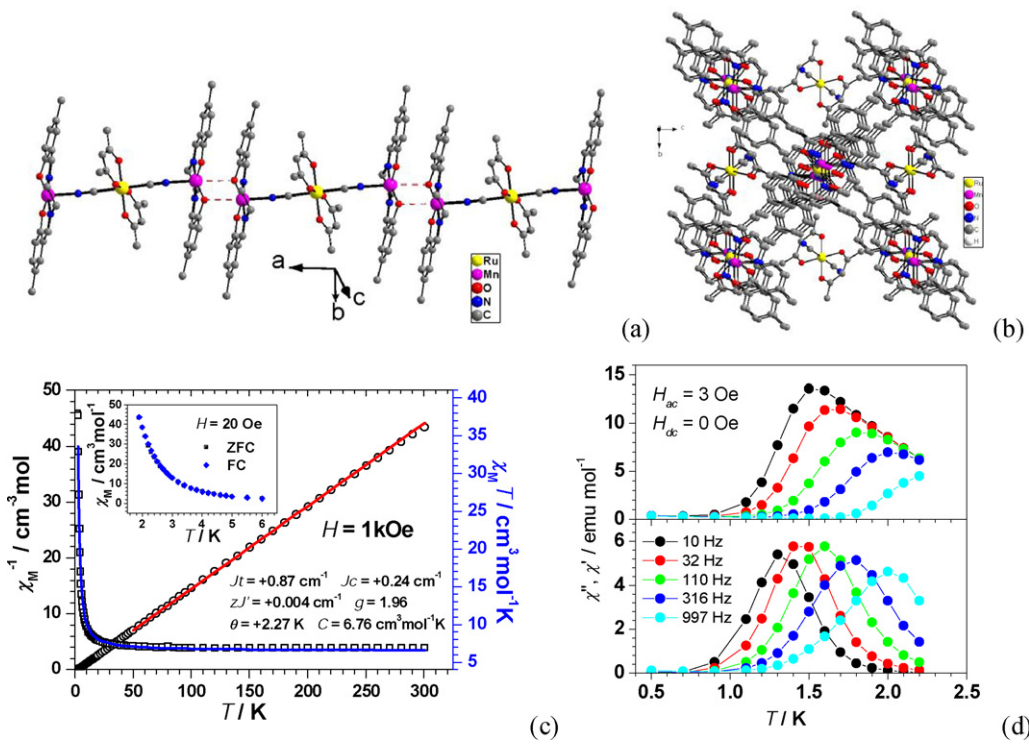


Fig. 9. 1D assembly of Mn³⁺-Ru³⁺-Mn³⁺ trinuclear units (a) and crystal packing (b) in **9**; (c) temperature dependence of $\chi_M T$ (squares) and χ_M^{-1} (circles). The inset is plots of ZFCM and FCM at 20 Oe; (d) temperature dependence of χ'_M and χ''_M of the ac susceptibility.

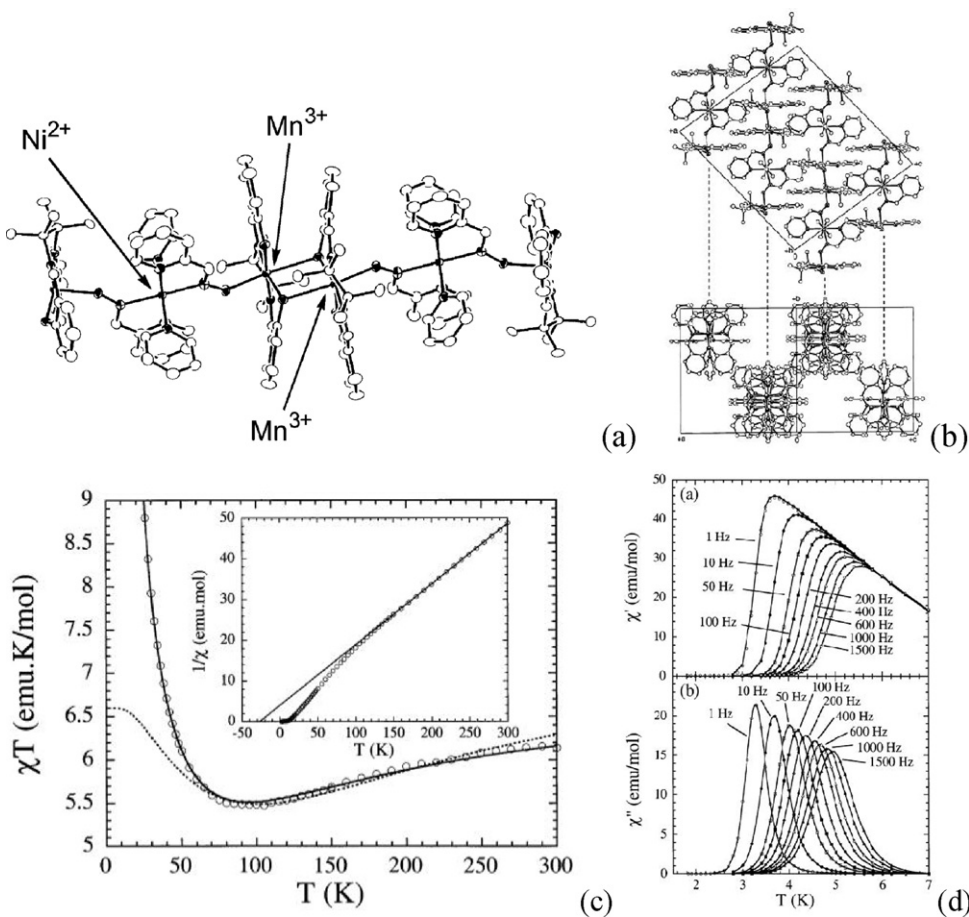


Fig. 10. Views of the crystal structure of $[\text{Mn}_2(\text{saltmen})_2\text{Ni}(\text{pao})_2(\text{py})_2](\text{ClO}_4)_2$ (**10a**) showing the heterometallic chain (a) and the chain packing in the crystal (b); (c) temperature dependence of the $\chi_M T$ and the fitting result by trimer Mn-Ni-Mn model; (d) temperature and frequency dependence of χ'_M and χ''_M of the ac susceptibility; reprinted with permission from Ref. [10a]. Copyright 2002 American Chemical Society.

antiferromagnetically coupled metal clusters. During the period of 2002–2008, Miyasaka et al. reported a series of 1D compounds (**10a–h**), in which Mn(saltmen) dimers are connected by $\text{Ni}(\text{pao})_2(\text{py})_2$ units [10]. The counter anions lie between the chains to separate the chains well (Fig. 10a and b). The dc magnetic measurements reveal dominant AF coupling between the spin carriers in these compounds. Because of weak FO interaction between the Mn^{3+} dimers and strong AF interaction transported by oximato group between Mn^{3+} and Ni^{2+} , these materials can be considered as an assembly of trimers ($\text{Mn}^{3+}\dots\text{Ni}^{2+}\dots\text{Mn}^{3+}$) with $\text{Mn}^{3+}\dots\text{Ni}^{2+}$ AF interactions (J) connected through weak J' interactions through phenolate oxygen bridge. Thus, the high-temperature magnetic data can be fitted by using a Heisenberg model considering the 1D arrangement of $[\text{Mn}^{3+}\dots\text{Ni}^{2+}\dots\text{Mn}^{3+}]$ trimers with strong intra-trimer couplings and weak inter-trimer ones. The fitted J/k_B values lie between -18.8 and -24.2 K and the J'/k_B in the range of 0.43 – 0.84 K [10]. The above fitting results clearly indicate that these 1D chain can be regarded as ferromagnetically coupled anisotropic $[\text{Mn}^{3+}\dots\text{Ni}^{2+}\dots\text{Mn}^{3+}]$ trimer ($S=3$). The ac susceptibility (temperature and frequency dependences) and dc (time relaxation of the magnetization and sweep rate dependent hysteresis loop) data demonstrate the existence of slow magnetic relaxation of SCM with a narrow distribution of relaxation times with α values between 0.05 and 0.15 (Table 1). Most of these materials display one relaxation process, with one relaxation time and energy barrier, except for $[\text{Mn}_2(\text{saltmen})_2\text{Ni}(\text{pao})_2(\text{py})_2](\text{ClO}_4)_2$ with two physical relaxation time and two corresponding different barriers, which is attributed to the effects of the chain finite-size [10a]. Interest-

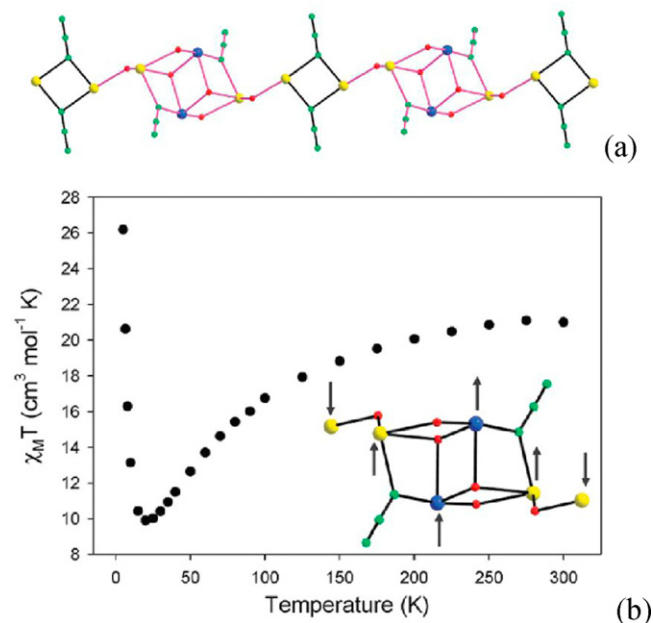


Fig. 11. (a) 1D chain found in **11**; (b) $\chi_M T$ vs. T plot in a 1 kOe field. Inset: proposed spin alignments in the repeating Mn₆ unit that give its putative $S=4$ ground state; reprinted with permission from Ref. [11]. Copyright 2009 American Chemical Society.

ingly, the correlation between the relaxation energy barrier ($\Delta E/k_B$) and the inter-trimer interaction J' value is linear according to the equation $\Delta E/k_B = 21 + 72J'/k_B$, reflecting the influence of magnetic interaction on relaxation barrier [10c].

In the above section, we discuss *FO* chains based on *FO* or *AF* coupled heterospin metal clusters. In 2009, Christou et al., reported another example of *FO* chain based on homospin clusters [11]. In $[\text{Mn}_6(\text{N}_3)_4(\text{O}_2\text{CMe})_2(\text{dpkd})_2(\text{dpkme})_2(\text{MeOH})_2]_n$ (11), the Mn_6 repeating units are bridged by *EO*-azido bridges to form a 1D chain structure (Fig. 11a). In each Mn_6 unit, the central planar $[\text{Mn}^{2+}_2\text{Mn}^{3+}_2]$ rhombus, which is bridged by $\mu_3\text{-OR}$ and $\mu_2\text{-OR}$, is connected on each side to two other Mn^{2+} by *EO*-azido and $\mu_2\text{-OR}$ bridges. The ferromagnetically coupled central rhombus with a resulting $S=9$ spin [34] and *AF* coupling between it and the two "extrinsic" Mn^{2+} atoms results in $S=4$ ground state for the Mn_6 unit. Hence the chain can be considered as consisting of ferromagnetically coupled anisotropic $S=4$ Mn_6 units (Fig. 11b). Further *ac* magnetic studies indicate the existence of slow magnetic relaxation with moderate distribution of relaxation time (Table 1).

3. Ferrimagnetic (*FI*) strategy towards SCM

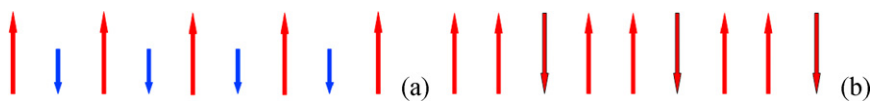
Compared with *FO* ground spin state, *AF* spin state is more stable and common in the field of molecular magnetism. *AF* coupling can also produce more interesting magnetic phenomena such as ferrimagnetism, weak ferromagnetism, metamagnetism and so on [26]. Among them, ferrimagnetism and weak ferromagnetism can be used to build SCM because these two spin

states can produce a net spin which is necessary for Glauber dynamics.

When two unequal spins are aligned in an antiparallel fashion, they will give net spins that are arranged in parallel, and this is one key factor for SCM. Another approach for *FI* chain is to combine *FO* and *AF* interaction which can also result in *FI* behavior [17]. Combined with some other factors required for SCM such as uniaxial anisotropy and weak interchain interaction, *FI* chain can ultimately become SCM. So far, several examples of *FI* SCM with different spin structures (Scheme 3), including the first SCM, $\text{Co}(\text{hfac})_2(\text{NITPhOMe})$, have been reported.

3.1. Organic radical-bridged ferrimagnetic SCM

The first one-dimensional compound, $\text{Co}(\text{hfac})_2(\text{NITPhOMe})$ (12), showing slow relaxation was reported in 2001 by the group of Gatteschi et al. [12]. Far from the prototype 1D topology imagined by Glauber, this compound is comprised of *FI* chains, in which $\text{Co}(\text{hfac})_2$ and NITPhOMe radical are alternately arranged in a helical chain (Fig. 12a). The strong uniaxial anisotropy of the Co^{2+} ions has been studied for 12 by susceptibility experiments performed upon a single crystal, and for the related mononuclear complex $\text{Co}(\text{hfac})_2(\text{NITPhOMe})_2$ by EPR and magnetic susceptibility measurements on single crystals [35]. The interaction between Co^{2+} and NITPhOMe radical is estimated to be *AF* ($J/k_B = -220\text{ K}$, $g_{\text{Co}} = 7.4$, $g_{\text{rad}} = 2$) by fitting the temperature dependence of $\chi_M T$ with an Ising model (Fig. 12b). The antiparallel arrangement of Co^{2+} ($S = 1/2$ and $g > 2$) and NITPhOMe radical ($S = 1/2$ and $g \approx 2$)



Scheme 3. Spin structures found in reported ferrimagnetic SCM.

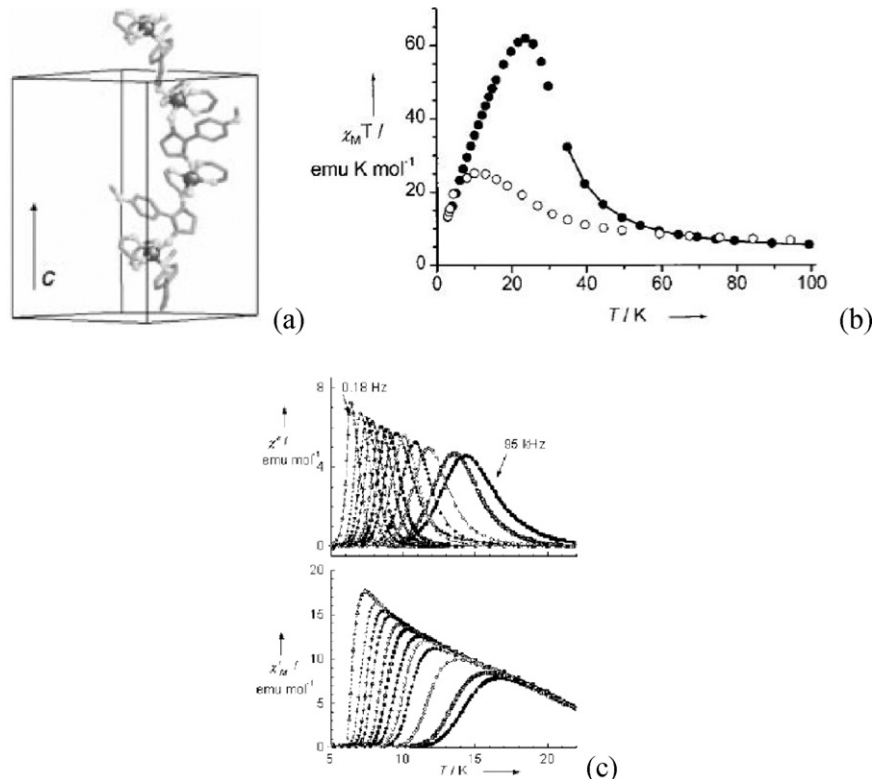


Fig. 12. (a) 1D helical chain in 12; (b) temperature dependence of $\chi_M T$ along or perpendicular to the chain direction; (c) temperature dependence of χ'_M and χ''_M of the *ac* susceptibility measured in zero applied static field; reprinted with permission from Ref. [12]. Copyright 2001 Wiley.

gives the non-compensative magnetic moments, resulting in a *FI* chain. The helical arrangement of the cobalt local anisotropy tensors leads to a complex magnetic behavior involving step features in the field dependence of the magnetization. At low temperature, slow relaxation of the magnetization is proved by strong frequency dependence of the *ac* data. The characteristic time of relaxation has been studied using different techniques: *ac* susceptibility, micro-SQUID magnetometer, NMR and μ SR (Fig. 12c) [36]. The relaxation time of $3.0(2) \times 10^{-11}$ s was deduced from an Arrhenius law with a gap $\Delta E/k_B = 153(2)$ K.

Interestingly, Ishida et al. reported an analogous derivative of $\text{Co}(\text{hfac})_2(\text{NITPhOMe})$ SCM with a slightly modified NITPh-O-R radical in which the original methyl group is substituted by a longer n-butyl group [37]. In $\text{Co}(\text{hfac})_2\text{BPNN}$, the change of radical also reduces the symmetry of the chain from threefold screw axis to binary screw axis, which makes the easy axis of the chain nearly parallel to each other and almost perpendicular to the chain. This situation favors *FO* dipolar interchain interaction, resulting in the magnetic ordering state. Studies of this compound as well as the first SCM clearly indicate the important role that interchain interaction plays in the construction of SCM.

Another example of *FI* SCM containing the organic radical TCNQ is reported by Miyasaka et al. in 2006 [13]. In $[\text{Mn}(5\text{-TMAMSaltmen})(\text{TCNQ})](\text{ClO}_4)_2$ (**13**), the $[\text{Mn}(5\text{-TMAMSaltmen})]$ moieties are bridged by TCNQ radicals in *trans-anti*-coordination fashion to form a zigzag chain structure. The counter ions ClO_4^- occupy the void space between the chains, to isolate the chains well (Fig. 13a and b). The *dc* magnetic measurement and the analysis of

the data between 30 and 300 K according to an alternating chain model of quantum spins, s_i , and classical spins S_i (also called the Seiden model) [38] indicate strong *AF* coupling between the Mn^{3+} and TCNQ radical with negative J/k_B value of -96.1 K (Fig. 13c). Consequently, this compound is made of strongly antiferromagnetically coupled $S_{\text{Mn}} = 2$: $S_{\text{Rad}} = 1/2$ *FI* 1D chains. The uniaxial anisotropy, with the easy axis along *c*-axis, was proved by magnetic measurement against single crystal. Below 10 K, strongly frequency dependence of *ac* susceptibilities was found for both the χ'_M and χ''_M signals, suggesting the presence of magnetic relaxation (Fig. 13d). The above mentioned data together with the heat-capacity measurements that show no λ peak rule out the possibility of a 3D ordering and spin glass-like behavior. Thus, the present magnetization dynamics suggest the occurrence of SCM behavior with a narrow distribution of relaxation time (Table 1). The relaxation time was determined by both *ac* data measured by a commercial SQUID apparatus and *dc* data by a home-made micro-SQUID magnetometer. These data follow the Arrhenius law and give two sets of relaxation time (2.1×10^{-10} s in high-temperature region and 6.8×10^{-6} s in low-temperature region) with two energy barrier (91.4 and 67.7 K), which are predicted when the correlation length becomes larger than the real chain length that can be limited by the structural defects.

3.2. Oxamate-bridged ferrimagnetic SCM

In 2004, Lloret et al. reported a Co^{2+} – Cu^{2+} bimetallic SCM $[\text{CoCu}(2,4,6\text{-tmpa})_2(\text{H}_2\text{O})_2] \cdot 4\text{H}_2\text{O}$ (**14**) [14]. In this compound, the

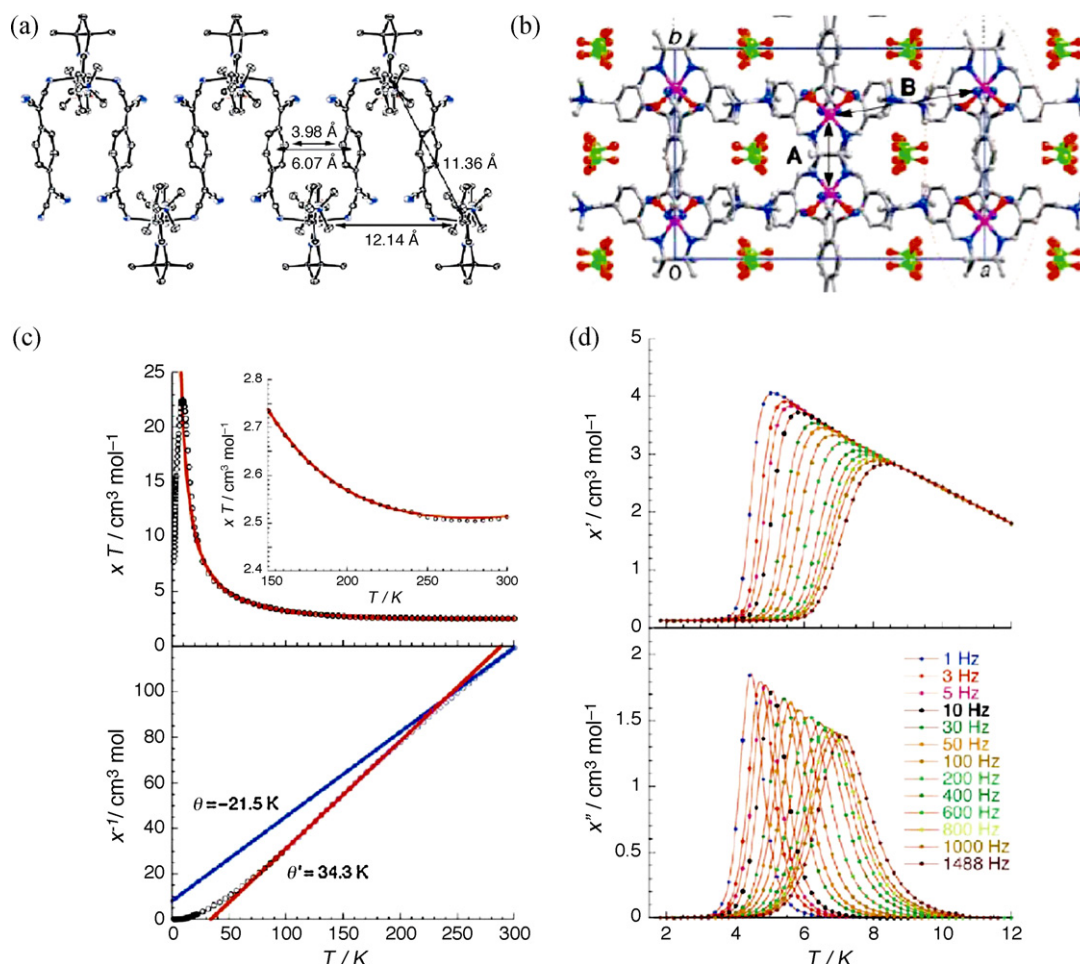


Fig. 13. The zigzag chain structure (a) and chain packing (b) in **13**; (c) temperature dependence of $\chi_M T$ and χ_M^{-1} and the good simulation results by using the Seiden model; (d) temperature dependence of the *ac* susceptibilities; reprinted with permission from Ref. [13]. Copyright 2006 Wiley.

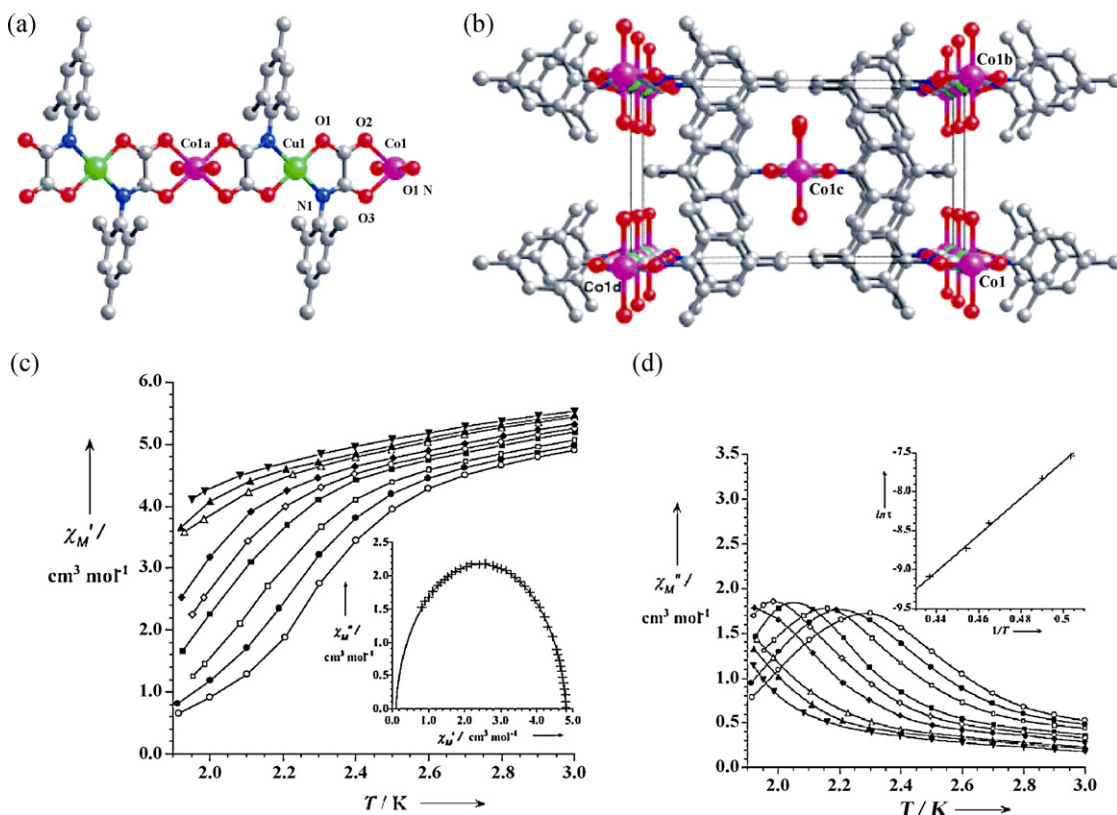


Fig. 14. The view of fragment of bimetallic chain (a) and the chain packing diagram (b) in **14**; temperature dependence of χ_M' (c) and χ_M'' (d) ac susceptibility; reprinted with permission from Ref. [14]. Copyright 2004 Wiley.

$\text{Cu}(\text{2,4,6-tmpa})_2^{2-}$ units are coordinated to Co^{2+} ions in a *trans* arrangement and bridge them to form 1D straight chain along *c*-axis with alternating arrangement of Cu^{2+} and Co^{2+} ions. The phenyl rings are nearly perpendicular to the oxamate groups, which afford effective magnetic shielding between neighboring chains in the *ab* plane. Along the *b*-axis, these chains are separated by some weak interchain hydrogen-bonding interactions between the coordinated and the lattice water molecules (Fig. 14a and b). *Dc* susceptibility measurements ($\chi_M T-T$ plots) show characteristic *Fl* behavior and analysis of the data with the consideration of single ion behavior of Co^{2+} and magnetic coupling leads to an estimation of the *AF* coupling ($J = -35 \text{ cm}^{-1}$, $g_{\text{Co}} = 2.38$, $g_{\text{Cu}} = 2.05$) between Co^{2+} and Cu^{2+} ions. The *ac* susceptibilities show clear frequency dependence and the fitting results by using Arrhenius law and generalized Debye model reveal the existence of single process slow magnetic relaxation (Fig. 14c and d and Table 1).

3.3. Cyanide-bridged ferrimagnetic SCM

In Section 2, we discussed *FO* SCM built by metal cyanide units. Cyanide can also transmit *AF* coupling, hence it can also be used for constructing SCM [26d]. In 2008, Hong et al. reported a cyanide-bridged *Fl* chain showing SCM behavior [15]. In the reported compound $[\text{W}(\text{CN})_6(\text{bpy})][\text{Mn}(\text{L}) \cdot \text{H}_2\text{O}]$ [15], $\text{L} = \text{N,N'-bis}(2\text{-hydroxynaphthalene}-1\text{-carbaldehydene}-trans-diaminocyclohexane]$, the MnL^{3+} units are bridged by $\text{W}(\text{CN})_6(\text{bpy})^-$ moieties to form a 1D linear chain structure (Fig. 15a). These chains are well separated by the phenoxide and benzene rings. The *dc* magnetic data clearly indicate typical *Fl* behavior in this compound. The fitting of the $\chi_M T-T$ data in the temperature range of 35–300 K by alternating chain model raised by Drillon et al. [39] affords estimated results of $g_{\text{Mn}} = 2.06$, $g_{\text{W}} = 2.14$, and $J = -11.8 \text{ cm}^{-1}$ (Fig. 15b). Further *ac* magnetic susceptibility measurements and

the fitting results by using Arrhenius equation and a generalized Debye model suggest the existence of single process slow magnetic relaxation of SCM (Table 1).

3.4. Other ligand-bridged ferrimagnetic SCM

In 2005, Kajiwara et al. reported another building block, $\text{M}(\text{bpca})_2^-$ ($\text{M} = \text{Cr}^{3+}, \text{Fe}^{3+}, \text{Co}^{3+}$), that can be used for constructing *Fl* chains [40]. A SCM, $[\text{Fe}(\text{ClO}_4)_2\{\text{Fe}(\text{bpca})_2\}\text{ClO}_4]$ [16], was synthesized by using this type of building block, in which the $\text{Fe}(\text{bpca})_2^-$ units are coordinated to Fe^{2+} ions in a *trans* arrangement and bridge them to form an alternating chain of Fe^{2+} and Fe^{3+} [16]. The Fe^{2+} ion adopts an axial elongated coordination geometry with four equatorial carbonyl oxygen atoms and two axial ClO_4^- oxygen atoms, which are expected to provide easy-plane-type anisotropy (Fig. 16a). The temperature dependence of the effective magnetic moment for microcrystalline sample is clearly consistent with the presence of a *Fl* ground state (Fig. 16b), and the *dc* data can be fitted by Heisenberg alternating $S=2, S=1/2$ chain model with consideration of the anisotropy of Fe^{2+} , giving $J/k_B = -10 \text{ K}$ and $D/k_B = +14.9 \text{ K}$. The single crystal magnetic measurement shows the presence of an easy axis along the chain, which is rationalized on the basis of the $\text{Fe}^{2+}/\text{Fe}^{3+}$ *AF* coupling and the orthogonal orientation of the two easy-plane anisotropic Fe^{2+} ions. Slow magnetic relaxation is observed, as suggested by the frequency dependence of the *ac* susceptibility data. Fitting of these *ac* susceptibilities using a generalized Debye and Arrhenius law indicates that the relaxation possess is a characteristic SCM one with a narrow distribution (Table 1).

3.5. Homospin ferrimagnetic SCM

Ferrimagnetism usually refers to heterospin systems. However, a homospin system with competitive interaction can also exhibit

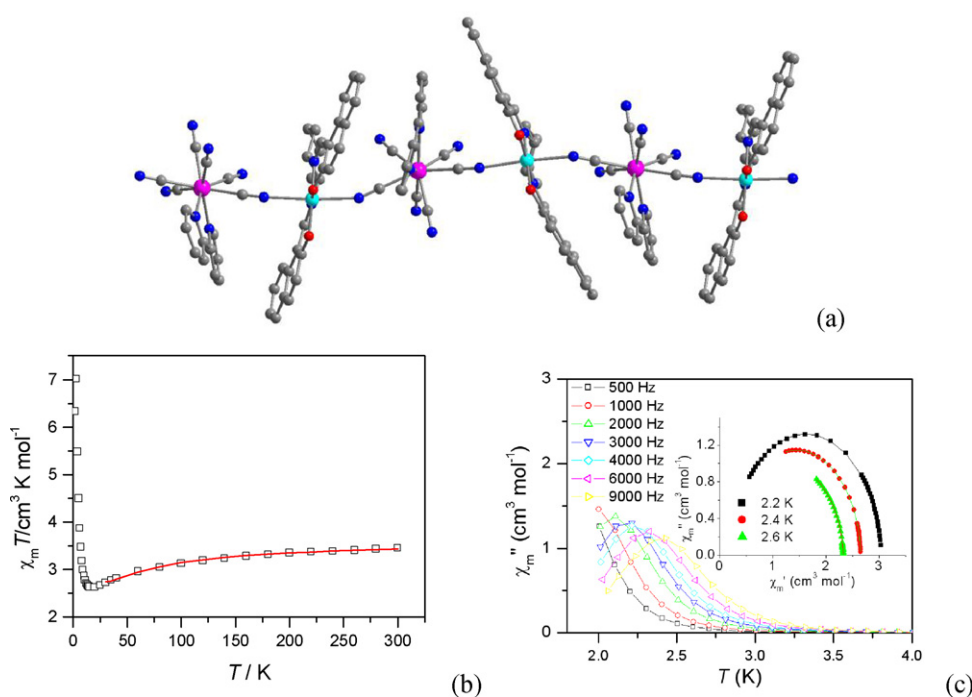


Fig. 15. (a) The view of chain structure in **15**; (b) temperature dependences of magnetic data together with the best fitting results; (c) χ''_M and Cole–Cole plots (inset) at indicated frequencies and temperatures, respectively; reprinted with permission from Ref. [15].

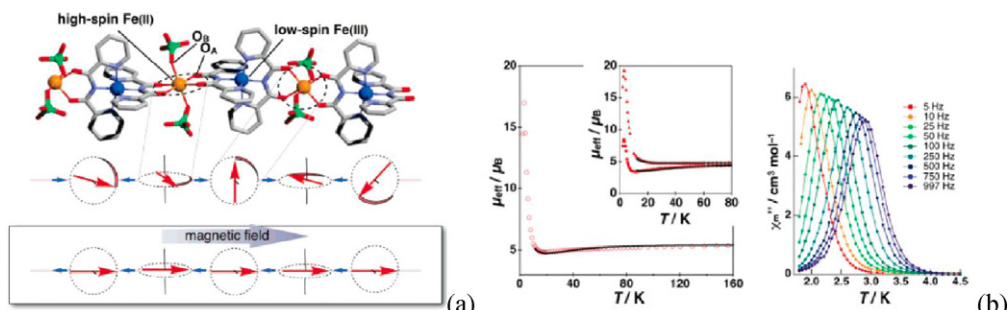


Fig. 16. (a) Crystal structure and spin arrangement of high-spin Fe^{2+} and low-spin Fe^{3+} alternating chain complex **16**. (b) (Left) Temperature dependence of μ_{eff} for the powder sample. (Inset) Magnetic measurements on an oriented single crystal along the chain and perpendicular to the chain. (Right) χ''_M vs. temperature under a zero dc field; reprinted with permission from Ref. [16]. Copyright 2005 American Chemical Society.

FI behavior [41]. In 2006, Gao and Cao et al. reported a homospin *FI* SCM, $[\text{Co}_3(\text{bime})_2(\mu_3-\text{OH})_2(\text{HO-BDC})_2]_n$ (**17**), in which the Co^{2+} ions are connected by alternating double μ_3 -OH and μ_2,η_3 -carboxylate bridges to form a 1D chain. Within the chain, two Co^{2+} ions bridged by double μ_3 -OH bridges are connected to one Co^{1+} ion to form trinuclear units, which are linked reversely through sharing of a μ_3 -OH, μ_2,η_3 -carboxylate and a gauche bime bridge to generate a 1D chain (Fig. 17a and b) [17a]. The chains are further extended into a 3D framework through the carboxylate group of HO-BDC with the shortest interchain $\text{Co}\cdots\text{Co}$ distance of 9.99 Å. As previously demonstrated for the cobalt hydroxyl derivatives [30a], the arrangement about the Co^{2+} centers sharing the μ_3 -OH groups are related to *FO* coupling, whereas *AF* exchanges occur between Co^{1+} and Co^{2+} . By considering the intrachain $\text{Co}\cdots\text{Co}$ distance and the magnitude of *AF* coupling transported by different bridges, the chain can be approximately simplified as a zigzag cobalt chain along $-\text{Co}^{2+}\text{A}-\text{Co}^{2+}\text{B}-\text{Co}^{1+}\text{C}-\text{Co}^{2+}\text{D}-$ with *FO/AF/AF* magnetic interactions.

With decreasing the temperature, the $\chi_M T$ first decreases gradually, reaches a minimum at about 69 K and then increases abruptly below 30 K, suggesting a *FI* character. The complicated chain is approximated as a zigzag cobalt chain along $-\text{Co}^{2+}\text{A}-\text{Co}^{2+}\text{B}-\text{Co}^{1+}\text{C}-\text{Co}^{2+}\text{D}-$

with alternating *FO/AF/AF* interactions to estimate the magnetic exchange between adjacent Co^{2+} ions. The $\chi_M T$ data above 40 K can be fitted well by an alternating 1D chain ($S=3/2$) model [$H=-J_1 \sum (S_{3i}S_{3i+1} + S_{3i+1}S_{3i+2}) - J_2 \sum S_{3i+1}S_{3i}$], where J_1 and J_2 are the intrachain coupling of $\text{Co}^{1+}/\text{Co}^{2+}$ and $\text{Co}^{2+}/\text{Co}^{2+}$, respectively; giving $J_1=-35.7(5)\text{ cm}^{-1}$, $J_2=+13.9(3)\text{ cm}^{-1}$, $g=2.528(8)$. The ferrimagnetic-like behavior is suggested to arise from the competitive *FO* coupling between Co^{2+} ions and the *AF* coupling between Co^{1+} and Co^{2+} ions, resulting in a net moment of one Co^{2+} ion per Co_3 unit. The *ac* magnetic susceptibility data show a strong frequency dependence in both χ'_M and χ''_M parts with a qualified ϕ value of 0.15 [32], suggesting the presence of superparamagnetic behavior (Fig. 17c). The Cole–Cole plots measured at 5.9 K can be fitted by a generalized Debye model with an α parameter of 0.50, indicating a large distribution in relaxation time. A relaxation time of 1.1×10^{-9} s is deduced from the *ac* data by Arrhenius law with energy barrier of 76(1) K. Interestingly, when applying a static *dc* field, the total *ac* susceptibility is divided into two peaks. One high-temperature frequency-independent peak and one low-temperature frequency-dependent peak are observed, indicating thermodynamic feature associated with finite-size effects (Fig. 17d) [42].

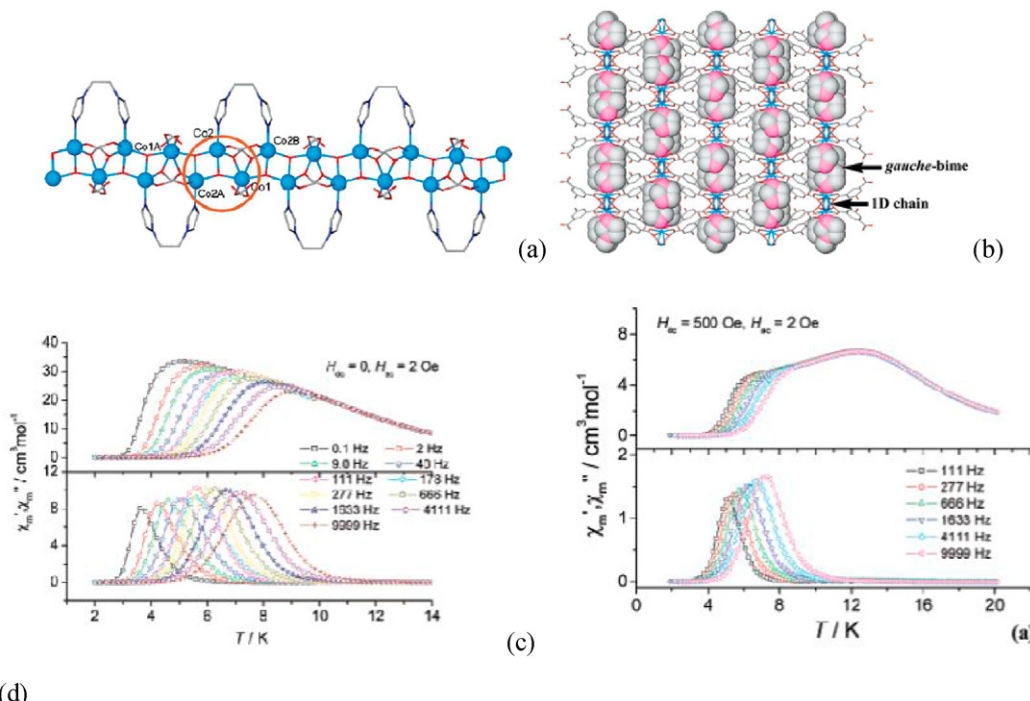


Fig. 17. (a) View of the 1D chain of **17**, with the trinuclear subunit exhibited in the orange loop; (b) view of a 3D framework derived from 1D chains linked by HO-BDC; temperature dependence of χ_M' and χ_M'' of the ac susceptibility in zero dc field (c) and 500 Oe (d). Copyright 2006 American Chemical Society.

4. Weak ferromagnetic (WF) strategy towards SCM

Another AF state which can be exploited to give SCM is the WF state. In this case the antiferromagnetically coupled moments make an angle different from 180° , resulting in an uncompensated moment (**Scheme 4**). Thus, AF chain with magnetic anisotropy is present, and if the easy axes are not collinear, it can ultimately show Glauber dynamics provided interchain interaction is weak enough. An useful strategy to get WF spin state is to employ asymmetric three-atom bridging ligands that favor non-collinear magnetic interaction. Furthermore, it is usual in molecular systems that the symmetry on the metal site is lower than that of the crystal space group and the 1D structure is generated by either a glide plane or a screw axis, thus inducing non-collinearity of the anisotropy axes [21]. However, WF SCM is relatively rare and only a few examples have been reported.

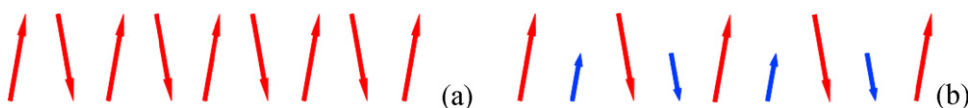
4.1. Phosphate-bridged weak ferromagnetic SCM

The first example of WF SCM, $\text{Co}(\text{H}_2\text{L})(\text{H}_2\text{O})$ [**18**, $\text{H}_4\text{L}=4\text{-Me-C}_6\text{H}_4\text{-CH}_2\text{N-(CPO}_3\text{H}_2\text{)}_2$], was reported by Mao and Dunbar in 2005, in which the antiferromagnetically coupled Co^{2+} chain exhibits SCM behavior [18]. The Co^{2+} ions adopt a tetragonal coordination environment. The doubly protonated pentadentate diphosphonate ligand acts as a tridentate ligand chelating to one Co^{2+} ion and as a bridge to independent Co^{2+} ions. One of the $-\text{PO}_3\text{H}$ group acts as tridentate ligand and one of its oxygen atom is a μ_2 bridge, which links Co^{2+} ions to form a 1D zigzag chain (**Fig. 18a**). The neighboring chains are well separated by both hydrogen bonds between phosphonate oxygen atoms and the $\text{Me-C}_6\text{H}_4\text{-CH}_2\text{-}$ sub-

stituents on the phosphonate groups. The overall shape of $\chi_M T$ vs. T plots is quite similar to that observed in AF spin chains (**Fig. 18b**). However, further magnetic analysis reveals that although the chain contains only antiferromagnetically coupled Co^{2+} ions, due to spin canting there is a resulting moment that is Ising in behavior. The magnetic exchange parameter $J=-10.5 \text{ cm}^{-1}$ is determined using the theoretical approach involving anisotropic exchange of Co^{2+} ions arranged in a linear chain with two alternating sites for magnetic ions. The strong uniaxial magnetic anisotropy arising from the tetragonal ligand fields acting on the Co^{2+} ions, the spin-orbit interaction, the AF exchange, and the topology of the chain are the main factors governing the spin-canting structure and subsequently to an uncompensated magnetic moment [18c]. Frequency-scan and temperature-scan measurements of the ac susceptibility reveal the presence of slow relaxation of the magnetization (**Fig. 18c** and d). The relaxation time extracted from these data follows an Arrhenius law with $\Delta E/k_B = 31.4 \text{ cm}^{-1} = 45.2 \text{ K}$; $\tau_0 = 1.13 \times 10^{-13} \text{ s}$ and $\Delta E/k_B \approx 18.6\text{--}20.2 \text{ cm}^{-1} = 26.8\text{--}29.1 \text{ K}$ and $\tau_0 \approx 8.4\text{--}34 \times 10^{-10} \text{ s}$ for temperature and frequency data, respectively. The semicircle Cole–Cole plots measured between 1.8 and 2.2 K can be fitted by a generalized Debye model with α value of 0.15–0.35, suggesting one relaxation process. According to the authors, the slow relaxation of SCM in **18** is induced by canting of the Co^{2+} spins along the chain which is supported by both experimental data and theoretical approach.

4.2. Organic radical-bridged weak ferromagnetic SCM

Besides transition metal ions, rare earth ions can also be used to construct SCM because of their Ising anisotropy. In 2005,



Scheme 4. Spin structures found in reported weak ferromagnetic SCM.

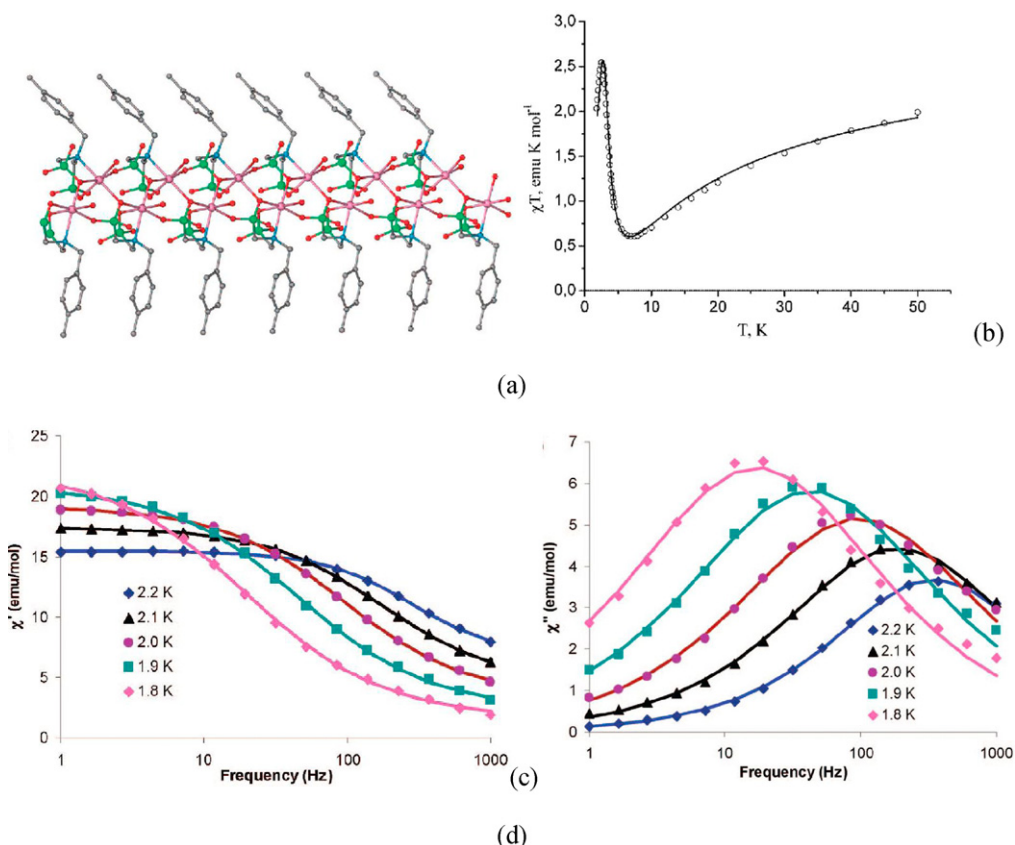


Fig. 18. (a) The view of the zigzag chain structure; (b) temperature dependence of $\chi_{\text{M}}T$ for **18**; frequency dependence of χ'_{M} (c) and χ''_{M} (d) of the *ac* magnetic susceptibility; reprinted with permission from Ref. [18c]. Copyright 2008 American Chemical Society.

Gatteschi et al. reported a 1D compound containing dysprosium and an organic radical with interesting dynamic properties [19]. Their work illustrates nicely how chemistry can be used to minimize the through space interchain interaction of a known system of $[\text{Dy}(\text{hfac})_3\text{NITEt}]$ with 3D magnetic ordering by modifying the radical moieties, in order to avoid the magnetic order for the benefit of a SCM behavior [43]. The NITEt radical was replaced by the bulky NITPhOPh derivative, resulting in the $[\text{Dy}(\text{hfac})_3\text{NITPhOPh}]$ compound with increasing interchain distances in all directions (Fig. 19a and b). As shown by the *dc* susceptibility measurements, this strategy is successful as no magnetic order is observed above 1.8 K. As suggested by the authors, the magnetism of this type of lanthanide–radical chain is characterized by the presence of nearest-neighbor (NN) *FO* metal–radical and next-nearest-neighbor (NNN) *AF* metal–metal or radical–radical magnetic couplings (J_{Mr} , J_{MM} , and J_{rr} , respectively) (Fig. 19c) [44]. The overall behavior at low temperature depends on the ratio between *FO* and *AF* interactions. The single crystal magnetic data and the *ab initio* estimation of the magnetic anisotropy of the Dy³⁺ ion based on the monomeric building block indicates weak 1D ferromagnetism along the chain axis and the NNN metal–metal *AF* interactions dominate [19c]. The transfer-matrix simulations by using a classical one-dimensional spin model with *AF* Heisenberg exchange interaction and non-collinear uniaxial single ion anisotropies favors a canted *AF* spin arrangement, with a net magnetic moment along the chain axis. Below 4.5 K, the *ac* magnetic susceptibility, measured in zero *dc* field, displays a frequency-dependent peak for both χ'_{M} and χ''_{M} signals, indicating the presence of slow magnetic relaxation with narrow distribution of relaxation (Fig. 19d, Table 1). The Arrhenius plot extracted from these data gives two different activated regimes with physical τ_0 values and

two different energy barriers (Table 1), indicating the existence of the finite-size effects. The substitution of some other rare earth ions (Tb³⁺, Ho³⁺) gives isostructural compounds with similar SCM magnetic behavior [19b]. Similar to the Dy complex, the Ho³⁺ complex also exhibits slow relaxation in two temperature regions with the finite-size effects. However, the Tb³⁺ compound exhibits a unique relaxation process [19b].

4.3. *EE*-azido-bridged weak ferromagnetic Ni²⁺ chain

In Section 2, we summarized the use of azide ligand in the construction of SCM due to its contribution to *FO* interaction found in *EO* bridging mode [2]. Actually, another bridging mode of azide (*EE*) can also be used to construct SCM because *EE*-azide can transmit *AF* coupling efficiently and some *EE*-azide containing WF materials have been reported [27]. In 2006, Gao et al. reported a *EE*-azide bridged WF chain compound, $[\text{Ni}(\mu\text{-N}_3)(\text{bmdt})(\text{N}_3)]_n(\text{DMF})_n$ (**20**), in which slow magnetic relaxation was observed [20]. In **20**, the Ni²⁺ ions are connected by a single *EE*-azido bridge to form a 1D chain, while the bulky bmdt helps to separate the chains in space (Fig. 20a and b). *Dc* magnetic measurements reveal strong *AF* interaction between Ni²⁺ ions and spin-canting behavior in the low-temperature region. The high-temperature $\chi_{\text{M}}T$ data can be fitted by uniform 1D $S=1$ chain model, giving $J=-16.0(7)\text{ cm}^{-1}$ and $g=2.30(1)$ (Fig. 20c). It seems that this compound fulfills the conditions required for SCM (the WF ground state, anisotropy of the Ni²⁺ ion and the larger interchain separation) and should show SCM magnetic behavior. However, the slow relaxation revealed by *ac* data is not simple Glauber dynamics as in a typical SCM. More studies are required to fully understand its relaxation behavior.

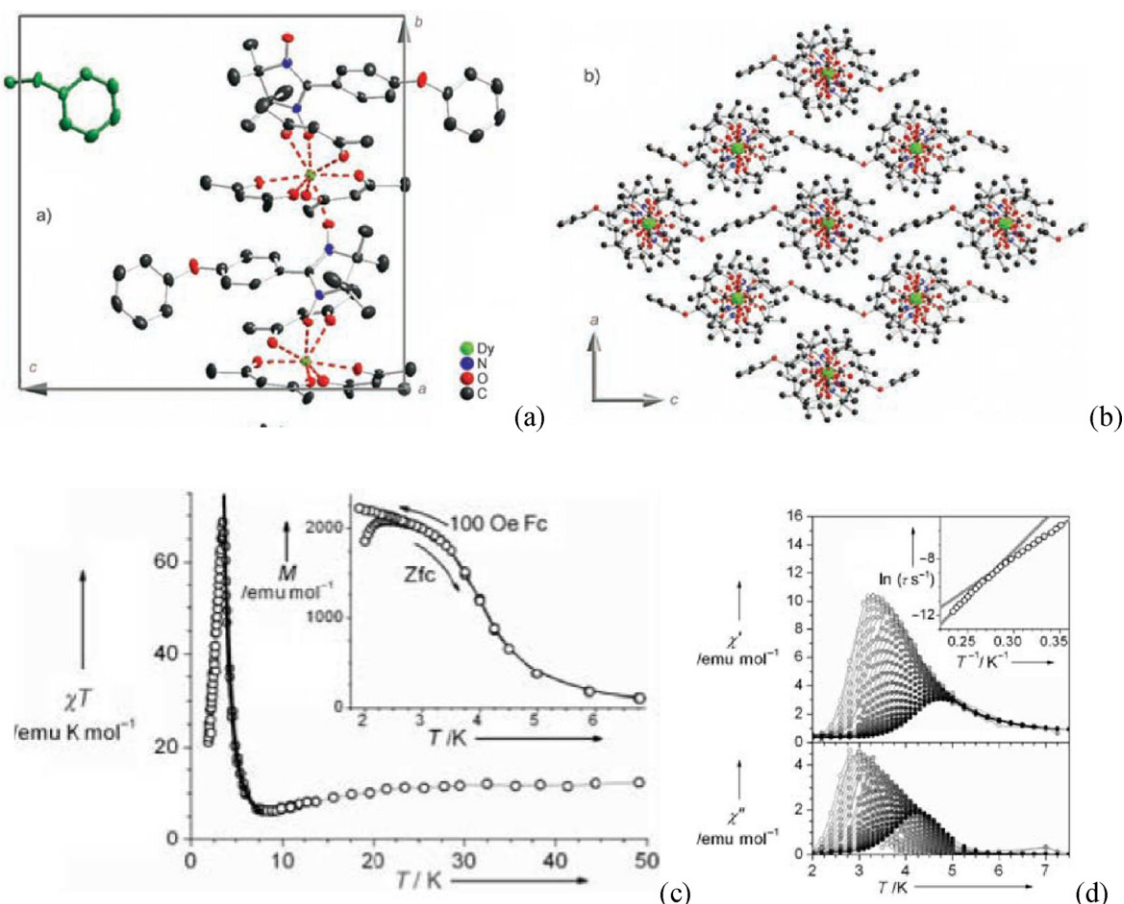


Fig. 19. Views of the structure of $[\text{Dy}(\text{hfac})_3\text{NITPhOPh}]$ (**19**): (a) along the *a*-axis, showing the chain structure together with the unit cell; (b) along the crystallographic *b*-axis, showing the packing of the chains; (c) low-temperature dependence of the χT product from *dc* magnetic measurements and the *ZFCM/FCM* plots; (d) temperature dependence of χ'_M and χ''_M of the *ac* magnetic susceptibility measured in zero applied field and the Arrhenius plot (inset); reprinted with permission from Ref. [19a]. Copyright 2005 Wiley.

4.4. Phosphinate-bridged weak ferromagnetic SCM

In 2008, Sessoli et al. synthesized another WF SCM, $[\text{Mn}(\text{TPP})\text{O}_2\text{PHPh}]\text{H}_2\text{O}$ (**21**) [21], by weakening the interchain magnetic interaction of magnetic ordered canted antiferromagnetic 1D system of $[\text{Mn}(\text{cyclam})\text{SO}_4]\text{ClO}_4\cdot\text{H}_2\text{O}$ [45]. In this compound, the Mn³⁺ ions adopt an elongated octahedral environment with their Jahn-Teller axis forming an angle of 21.01° with the crystallographic *c*-axis. The Mn-porphyrin moieties connected by the phosphinate ligands form infinite $[\text{Mn}-\text{O}-\text{P}-\text{O}]_n$ zigzag chains along the crystallographic *c*-axis generated by the glide plane symmetry element. The adjacent chains are parallelly packed along *c*-axis, displaying a hexagonal-type arrangement (Fig. 21a and b).

The overall shape of $\chi_M T$ vs. *T* plots displays the typical behavior of AF 1D structure in the presence of spin canting (Fig. 21c). The rotation magnetic measurements on single crystal samples indicate that the three principal magnetic axes for magnetic anisotropy are crystallographic *a*-, *b*-, and *c*-axis, respectively. Further temperature or field dependence of single crystals magnetic data suggests that *a*-axis is the easy axis and the uncompensated moments are arranged along the *b*-axis. The fitting of these data by Monte Carlo calculations gives *J* = 0.68(4) K, *D* = −4.7(2) K, and *g* = 1.97(1), which clearly indicates that the AF interaction transmitted by phenylphosphinate combined with the easy axis magnetic anisotropy of the Mn³⁺ sites give rise to a canted AF arrangement of the spins. The *ac* magnetic data are measured on an oriented sample constituted by aligned single crystals in three principal directions

and the susceptibility along the *b*-axis is much stronger than that along the other two axes, which is consistent with that found in *dc* magnetic measurement below 6 K (Fig. 21d). Along the *b*-axis, the intensity of χ''_M signal is comparable with that of χ'_M and both of them show clear frequency dependence, indicating typical SCM behavior. The temperature dependences of the *ac* susceptibility measured on a powder sample are close to what is observed along the *b*-axis. The values of the energy barrier, $\Delta E/k_B$, and the relaxation time, τ_0 , extracted from the powder sample measurements are equal to 36.8(6) K and $1.6(4) \times 10^{-10}$ s, respectively. Single crystal data taken along the *b*-axis provide similar parameters [$\Delta E/k_B$ = 34.6(9) K and τ_0 = $3.5(5) \times 10^{-10}$ s], which are comparable with those found in superparamagnetic systems. The semicircle Cole-Cole plots are found for both aligned single crystal and powder sample. The fitting of these data by a generalized Debye model gives quite small α value (0.014 at 3.2 K, 0.076 at 2.5 K for powder; 0.085 at 3.2 K and 0.1 at 2.5 K for single crystal), suggesting the single relaxation process. Interestingly, the application of a static magnetic field of 1 kOe has no sizable effects on the dynamic parameters.

4.5. Tetrazolate-bridged weak ferromagnetic SCM

Porous magnetic materials with rod packing structures can be good candidates for SCM because in these structures the magnetic chains are separated by other diamagnetic bridging ligands, which is the condition required by SCM. In 2009, Dunbar and Zubietta reported a tetrazolate bridged porous magnetic materials which

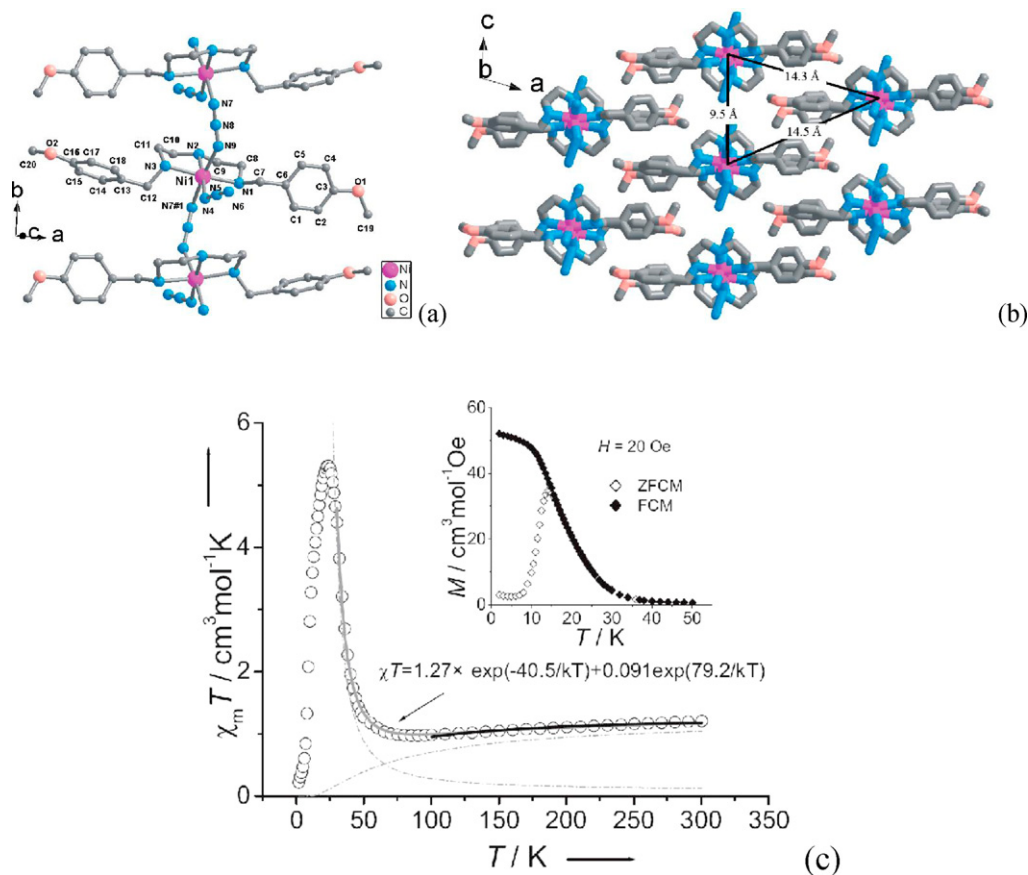


Fig. 20. (a) View of the 1D chain structure of **20** along the *b*-axis; (b) crystal packing in the *ac* plane; (c) temperature dependence of the magnetic susceptibility and the ZFCM and FCM (inset). Copyright 2006 Wiley.

show SCM magnetic behavior [22]. In $[\text{Co}_2(\text{H}_{0.67}\text{bdt})_3]\cdot 20\text{H}_2\text{O}$ (**22**), the Co^{2+} ions are connected by triple tetrazolate units to form $\{\text{Co}(\text{tetrazolate})_3\}_n$ chains along the crystallographic *a*-axis and these chains are further linked through the phenyl tethers of the bdt ligands into a 3D porous framework with channels of approximate dimensions $12.0\text{ \AA} \times 9.0\text{ \AA}$ (Fig. 22a–c). As the temperature is lowered, the *dc* magnetic data, shown in $\chi_M T$ – T plots, indicate that $\chi_M T$ first decreases to reach a minimum and increases at lower temperature, displaying the typical behavior of *AF* 1D structure in the presence of spin canting. The data above 50 K were fit to the 1D Fisher model and the best fitting gives $J = -2.55\text{ cm}^{-1}$ and $g = 2.9$. Slow magnetic relaxation expected for SCM was found in *ac* magnetic data, which show strong frequency dependence below 5 K with a qualified ϕ value of 0.14 (Fig. 22d). The relaxation time and the distribution of relaxation time (Table 1) can be extracted from *ac* data are comparable with that found in other reported SCMs.

Interestingly, the absorption and desorption of guest water molecules greatly affects its magnetic behavior (from SCM to paramagnetic materials with *AF* coupling). Thus it may be possible to control and/or tune the SCM magnetic behavior of such type of porous magnetic materials by including different guest molecules, which provides another way to control the interchain magnetic interaction of SCM [46]. These studies are of great interest because it will provide more insight in the design of SCM.

4.6. Weak ferromagnetic SCM based on $[\text{Mn}_3\text{O}]$ unit

From 2006 to 2009, Tao et al. reported step-by-step synthesis of a series SCM based on trinuclear building blocks $[\text{Mn}_3\text{O}]$ (Fig. 23) [23]. In $[\text{Mn}_3\text{O}]$ building blocks, the Mn^{3+} ions bridged by

pyrazole or oximate are antiferromagnetically coupled, resulting in a $S = 1$ frustrated state [47]. These $[\text{Mn}_3\text{O}]$ are further connected by *anti-anti* carboxylic or *EE*-azide group, forming 1D structures. These chains are well isolated from each other by the bulk alkyl groups of the ligands or the coordinated ethanol molecules. The overall magnetic interaction within the chain is *AF*, which is proved by both the shape of the $\chi_M T$ – T plots and the fitting of high-temperature magnetic data by the theoretical expression for an isosceles triangle model, with the addition of an interunit interaction by the mean-field approximation. The increase of the $\chi_M T$ value at low temperature is due to the spin-canting phenomenon. The *ac* magnetic susceptibility measured at zero *dc* field show strong frequency dependence with qualified ϕ value of 0.14–0.17, indicating the existence of slow magnetic relaxation. The relaxation time ($(3.7\text{--}12) \times 10^{-11}\text{ s}$) and the energy barrier (39.9–96.6 K) deduced from the frequency dependence of the peak temperatures of χ''_M are comparable with that found in other reported SCMs. Besides the observation of SCM behavior and various interesting phenomena, this series of compounds with similar structures provide us a chance to systematically explore the factors governing their magnetic behavior. Tao's SCM crystallizes in non-centric space groups and belongs to a class of dipole chains, which provide a suitable model for studying the dielectric relaxation in the time domain and the frequency domain by using Glauber dynamics on the kinetic Ising model [23a]. Furthermore, the existence of both magnetic relaxation and dielectric relaxation in one compound also provides the possibility for exploring the interaction between these two relaxation processes, which is the frontier in molecule based multi-functional materials. Our two SCM with similar $[\text{Mn}_3\text{O}]$ moieties but different bridging ligands show different blocking

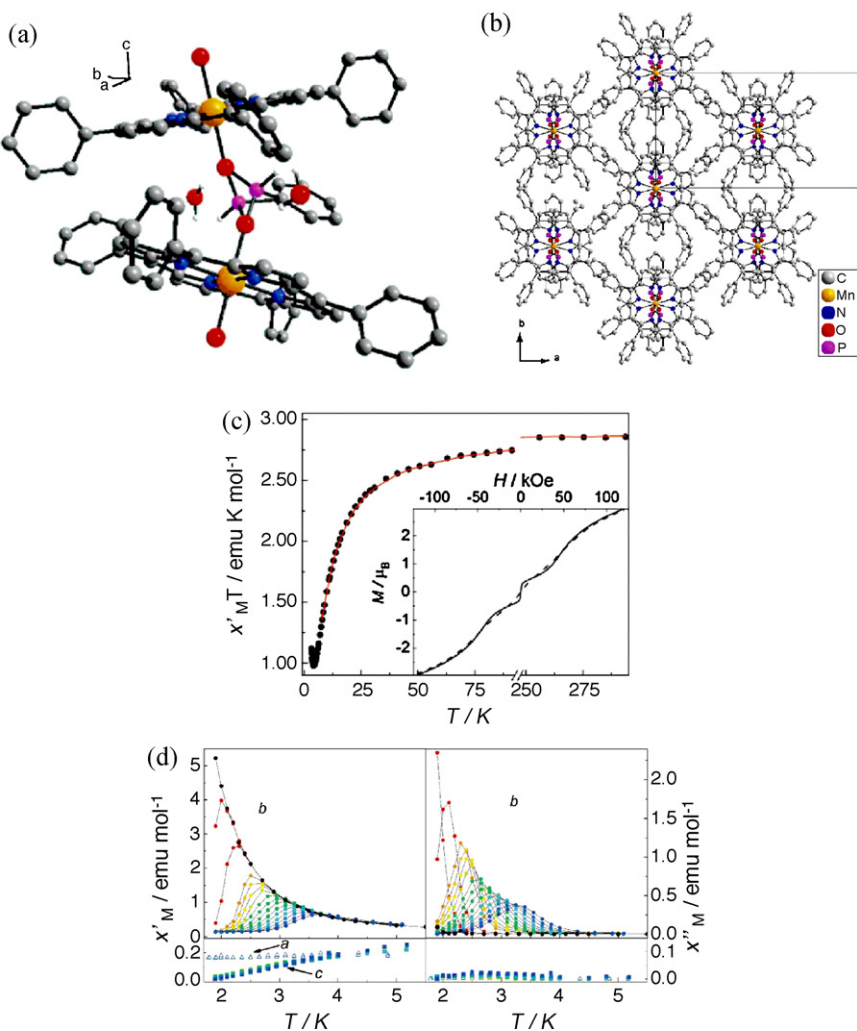


Fig. 21. (a) Two MnTPP complexes linked by the phenylphosphinato bridge; (b) crystal packing for **21** viewed along *c*-axis; (c) $\chi_M T$ vs. *T* of the powder susceptibility. The red line corresponds to the calculated susceptibility. In the inset the magnetization against field for the powder sample at 1.6 K (full line) and 4 K (dashed line) is reported; (d) plot of χ'_M and χ''_M against the temperature measured in zero static field. The crystals are oriented along *a* (open triangles), *b* (circles), and *c* (squares) axis; reprinted with permission from Ref. [21]. Copyright 2008 American Chemical Society.

temperatures of SCM, which clearly indicate the influence of intra-chain magnetic coupling on the overall magnetic behavior [23b]. $[\text{Mn}_3\text{O}(\text{tBusao})_3\text{N}_3(\text{CH}_3\text{OH})_4]\cdot0.5\text{CH}_3\text{OH}$ (**23b**), which is connected by the stronger magnetic coupler *EE*-azido, shows higher blocking

temperature and higher energy barrier of 96.6 K. Liu's paper gives us insight on how to obtain SCM through weakening the interchain interaction of 3D ordering systems and the influence of interchain interaction on SCM's blocking temperature [23c].

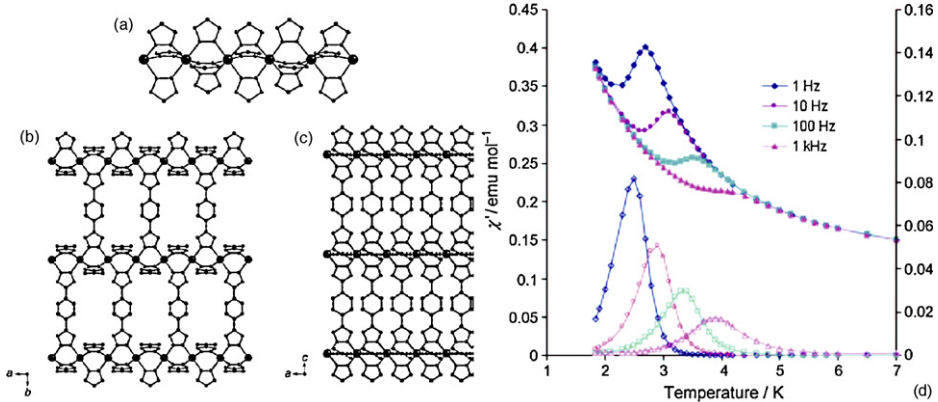


Fig. 22. (a) Ball-and-stick representation of the $\{\text{Co}(\text{tetrazolate})\}_n$ chain substructure of **22**; views of the linking of chains through the phenyl tether of the bdt ligand in the *ab* (b) and *bc* (c) plane; (d) temperature dependences of χ'_M and χ''_M of the *ac* magnetic susceptibility; reprinted with permission from Ref. [22]. Copyright 2009 Wiley.

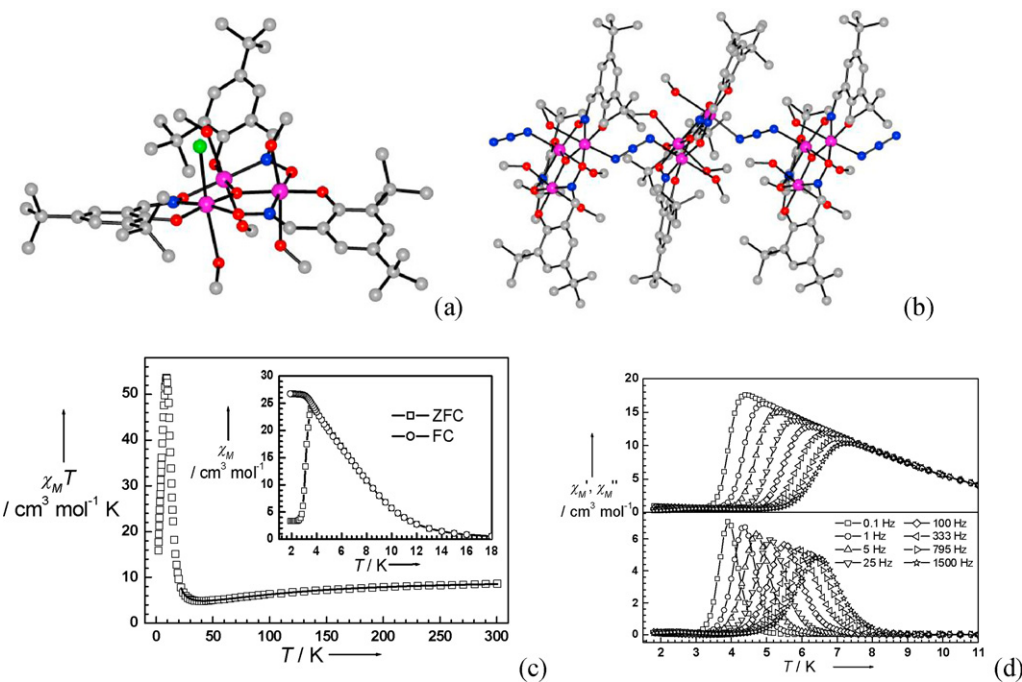


Fig. 23. (a) The molecular structure of $[Mn_3O]$; (b) the chain of $[Mn_3O]$ units bridged by N_3^- ions; temperature dependence dc (c) and ac (d) magnetic data for **23b**. Copyright 2007 Wiley.

5. Conclusion and perspective

In conclusion, we have demonstrated the success of three approaches, *FO*, *FI* and *WF*, to SCMs by typical examples. Our survey of this subject reveals that there are more *FO* SCMs than *FI* and *WF* ones, and this seems inverse to the 3D magnetic LRO systems. In *FO* SCMs, the *FO* interactions are mainly transmitted by the phenolate oxygen bridge between Mn^{3+} Schiff base units, *EO*-azide, cyanide and oxalate groups. For the former two bridges, the mechanism of *FO* coupling is clear. However, the fact that cyanide and oxalate transmits *FO* coupling between Fe^{3+} – Mn^{3+} and Cr^{3+} – Co^{2+} is not consistent with the orthogonal rule raised by Kahn, hence the mechanism needs further investigation. In addition, examples of SCM based on *FI* strategy are less than that expected from 3D ferrimagnets. This is probably due to the avoidless interchain interactions in 1D *FI* chain compounds, resulting in 3D ordering and metamagnetic behavior for *FO* and *AF* interchain interactions, respectively [48]. Therefore new *FI* SCM may be prepared by weakening the interchain interaction by adopting larger separators or other tuning methods. Another promising area in *FI* SCM is topological *FI* systems with competing interaction. Further study could provide new homospin *FI* SCM with new spin topology. Compared with *FO* or *FI* SCMs, *WF* SCMs are reported later; however, its number is increasing rapidly. In the future, we believe that more *WF* SCMs will be reported because it is easy to induce the non-collinearity of anisotropy axes due to the fact that asymmetric bridging modes and irregular coordination environment of anisotropic spin carriers are always found in the reported molecular systems.

Although SCM have potential applications as memory devices and record media, their blocking temperatures are still too low at the moment. The first prospective goal in the synthesis of SCM is to raise the blocking temperature. The promising method to increase the blocking temperature is to enhance the intrachain coupling by choosing stronger magnetic intermediators. However, it seems difficult to raise J too much because the values found in some reported SCMs are already quite high, such as 220 K for Co^{2+} -radical.

Another approach is to increase the uniaxial anisotropy by using spin carriers such as rare earth ions or 4d and 5d metal ions with stronger spin-orbital coupling or controlling the alignment of the easy axis of the spin carriers within the chain so as to enhance the bulky anisotropy for individual molecular chain. The later approach to increase the uniaxial anisotropy seems to be more interesting because it will provide some clues to understand how different spin topologies can afford higher blocking temperatures and the reported SCM usually have non-collinear local magnetization axes.

The second prospective goal is to create multi-functional SCM, in which the 1D magnetic behavior is coupled with other physical and/or chemical properties. Although some pioneering work on multi-functional SCM with optical second-harmonic generation properties, porous properties (porous SCM) and dielectric relaxation has been reported, multi-functional SCM with electronic conductivity (conductive SCM), optic properties (photoswitchable SCM) and chirality (chiral SCM) have not been created. Hence, design of magnetic chains with building blocks exhibiting various physical properties should provide systems to explore the interaction between physical properties as well as to study the influence of interchain magnetic interaction on the final behavior of SCM.

The third prospective goal is to organize SCM on substrates, which is a basic problem for chemists and surface scientists. Success in this area could lead to a better understanding of the role of the environment on SCM. And this might result in new application of SCM, such as a candidate for molecular spintronics.

Acknowledgements

We thank the financial support from the National Natural Science Foundation of China (Grants 20821091, 20801006, 90922033), the National Basic Research Program of China (Grants 2006CB601102, 2009CB929403). We also thank Prof. T.C. Lau in City University of Hong Kong for useful discussion and our co-workers for their distinct contributions.

References

- [1] (a) C. Coulon, H. Miyasaka, R. Clerac, *Struct. Bonding* 122 (2006) 163;
 (b) R. Lescouezec, L.M. Toma, J. Vaissermann, M. Verdaguer, F.S. Delgado, C. Ruiz-Perez, F. Lloret, M. Julve, *Coord. Chem. Rev.* 249 (2005) 2691;
 (c) L. Bogani, A. Vindigni, R. Sessoli, D. Gatteschi, *J. Mater. Chem.* 18 (2008) 4750.
- [2] (a) T.F. Liu, D. Fu, S. Gao, Y.Z. Zhang, H.L. Sun, G. Su, Y.J. Liu, *J. Am. Chem. Soc.* 125 (2003) 13976;
 (b) H.L. Sun, Z.M. Wang, S. Gao, *Chem. Eur. J.* 15 (2009) 1757.
- [3] (a) Y.Z. Zheng, M.L. Tong, W.X. Zhang, X.M. Chen, *Angew. Chem., Int. Ed.* 45 (2006) 6310;
 (b) Y.Z. Zheng, W. Xue, M.L. Tong, X.M. Chen, S.L. Zheng, *Inorg. Chem.* 47 (2008) 11202.
- [4] N. Shaikh, A. Panja, S. Goswami, P. Banerjee, P. Vojtisek, Y.Z. Zhang, G. Su, S. Gao, *Inorg. Chem.* 43 (2004) 849.
- [5] (a) F. Chang, S. Gao, H.L. Sun, Y.L. Hou, G. Su, Proceeding of the ICSM 2002 Conference (June 29–July 5th 2002), Fudan University, Shanghai, China, 2002, p. 182;
 (b) R. Lescouezec, J. Vaissermann, C. Ruiz-Perez, F. Lloret, R. Carrasco, M. Julve, M. Verdaguer, Y. Dromzee, D. Gatteschi, W. Wernsdorfer, *Angew. Chem., Int. Ed.* 42 (2003) 1483;
 (c) L.M. Toma, R. Lescouezec, J. Pasan, C. Ruiz-Perez, J. Vaissermann, J. Cano, R. Carrasco, W. Wernsdorfer, F. Lloret, M. Julve, *J. Am. Chem. Soc.* 128 (2006) 4842.
- [6] (a) S. Wang, J.L. Zuo, S. Gao, Y. Song, H.C. Zhou, Y.Z. Zhang, X.Z. You, *J. Am. Chem. Soc.* 126 (2004) 8900;
 (b) H.R. Wen, C.F. Wang, Y. Song, S. Gao, J.L. Zuo, X.Z. You, *Inorg. Chem.* 45 (2006) 8942.
- [7] E. Coronado, J.R. Galan-Mascaros, C. Martí-Gastaldo, *J. Am. Chem. Soc.* 130 (2008) 14987.
- [8] M. Ferbinteanu, H. Miyasaka, W. Wernsdorfer, K. Nakata, K. Sugiura, M. Yamashita, C. Coulon, R. Clerac, *J. Am. Chem. Soc.* 127 (2005) 3090.
- [9] J.F. Guo, X.T. Wang, B.W. Wang, S. Gao, L. Szeto, W.T. Wong, W.Y. Wong, T.C. Lau, *Chem. Eur. J.* Published Online: Feb 5 2010, doi:10.1002/chem.200902047.
- [10] (a) R. Clerac, H. Miyasaka, M. Yamashita, C. Coulon, *J. Am. Chem. Soc.* 124 (2002) 12837;
 (b) H. Miyasaka, R. Clerac, K. Mizushima, K. Sugiura, M. Yamashita, W. Wernsdorfer, C. Coulon, *Inorg. Chem.* 42 (2003) 8203;
 (c) A. Saitoh, H. Miyasaka, M. Yamashita, R. Clerac, *J. Mater. Chem.* 17 (2007) 2002;
 (d) H. Miyasaka, A. Saitoh, M. Yamashita, R. Clerac, *Dalton Trans.* (2008) 2422.
- [11] T.C. Stamatatos, K.A. Abboud, W. Wernsdorfer, G. Christou, *Inorg. Chem.* 48 (2009) 807.
- [12] A. Caneschi, D. Gatteschi, N. Lalioti, C. Sangregorio, R. Sessoli, G. Venturi, A. Vindigni, A. Rettori, M.G. Pini, M.A. Novak, *Angew. Chem., Int. Ed.* 40 (2001) 1760.
- [13] H. Miyasaka, T. Madanbashi, K. Sugimoto, Y. Nakazawa, W. Wernsdorfer, K. Sugiura, M. Yamashita, C. Coulon, R. Clerac, *Chem. Eur. J.* 12 (2006) 7028.
- [14] (a) E. Pardo, R. Ruiz-Garcia, F. Lloret, J. Faus, M. Julve, Y. Journaux, F.S. Delgado, C. Ruiz-Perez, *Adv. Mater.* 16 (2004) 1597;
 (b) E. Pardo, R. Ruiz-Garcia, F. Lloret, J. Faus, M. Julve, Y. Journaux, M.A. Novak, F.S. Delgado, C. Ruiz-Perez, *Chem. Eur. J.* 13 (2007) 2054.
- [15] S.W. Choi, H.Y. Kwak, J.H. Yoon, H.C. Kim, E.K. Koh, C.S. Hong, *Inorg. Chem.* 47 (2008) 10214.
- [16] (a) T. Kajiwara, M. Nakano, Y. Kaneko, S. Takaishi, T. Ito, M. Yamashita, A. Igashira-Kamiyama, H. Nojiri, Y. Ono, N. Kojima, *J. Am. Chem. Soc.* 127 (2005) 10150;
 (b) H. Tanaka, T. Kajiwara, Y. Kaneko, S. Takaishi, M. Yamashita, *Polyhedron* 26 (2007) 2105.
- [17] (a) X.J. Li, X.Y. Wang, S. Gao, R. Cao, *Inorg. Chem.* 45 (2006) 1508;
 (b) S. Hu, L. Yun, Y.Z. Zheng, Y.H. Lan, A.K. Powell, M.L. Tong, *Dalton Trans.* (2009) 1897.
- [18] (a) Z.M. Sun, A.V. Prosvirin, H.H. Zhao, J.G. Mao, K.R. Dunbar, *J. Appl. Phys.* 97 (2005) 10B305;
 (b) A.V. Palii, S.M. Ostrovsky, S.I. Klokishner, O.S. Reu, Z.M. Sun, A.V. Prosvirin, H.H. Zhao, J.G. Mao, K.R. Dunbar, *J. Phys. Chem. A* 110 (2006) 14003;
 (c) A.V. Palii, O.S. Reu, S.M. Ostrovsky, S.I. Klokishner, B.S. Tsukerblat, Z.M. Sun, J.G. Mao, A.V. Prosvirin, H.H. Zhao, K.R. Dunbar, *J. Am. Chem. Soc.* 130 (2008) 14729.
- [19] (a) L. Bogani, C. Sangregorio, R. Sessoli, D. Gatteschi, *Angew. Chem., Int. Ed.* 44 (2005) 5817;
- (b) K. Bernot, L. Bogani, A. Caneschi, D. Gatteschi, R. Sessoli, *J. Am. Chem. Soc.* 128 (2006) 7947;
 (c) K. Bernot, J. Luzon, A. Caneschi, D. Gatteschi, R. Sessoli, L. Bogani, A. Vindigni, A. Rettori, M.G. Pini, *Phys. Rev. B* 79 (2009) 134419.
- [20] X.T. Liu, X.Y. Wang, W.X. Zhang, P. Cui, S. Gao, *Adv. Mater.* 18 (2006) 2852.
- [21] K. Bernot, J. Luzon, R. Sessoli, A. Vindigni, J. Thion, S. Richeter, D. Leclercq, J. Larionova, A. Lee, *J. Am. Chem. Soc.* 130 (2008) 1619.
- [22] W. Ouellette, A.V. Prosvirin, K. Whitenack, K.R. Dunbar, J. Zubietta, *Angew. Chem., Int. Ed.* 48 (2009) 2140.
- [23] (a) Y.L. Bai, J. Tao, W. Wernsdorfer, O. Sato, R.B. Huang, L.S. Zheng, *J. Am. Chem. Soc.* 128 (2006) 16428;
 (b) H.B. Xu, B.W. Wang, F. Pan, Z.M. Wang, S. Gao, *Angew. Chem., Int. Ed.* 46 (2007) 7388;
 (c) C.M. Liu, D.Q. Zhang, D.B. Zhu, *Inorg. Chem.* 48 (2009) 4980.
- [24] (a) R. Sessoli, D. Gatteschi, A. Caneschi, M.A. Novak, *Nature* 365 (1993) 141;
 (b) R. Sessoli, H.L. Tsai, A.R. Schake, S. Wang, J.B. Vincent, K. Folting, D. Gatteschi, G. Christou, D.N. Hendrickson, *J. Am. Chem. Soc.* 115 (1993) 1804.
- [25] R.J. Glauber, *J. Math. Phys.* 4 (1963) 294.
- [26] (a) O. Kahn, *Molecular Magnetism*, VCH Publisher, 1992;
 (b) R.L. Carlin, *Magnetochemistry*, Springer-Verlag, 1986;
 (c) H.Z. Kou, S. Gao, J. Zhang, G.H. Wen, G. Su, R.K. Zheng, X.X. Zhang, *J. Am. Chem. Soc.* 123 (2001) 11809;
 (d) S.M. Holmes, G.S. Girolami, *J. Am. Chem. Soc.* 121 (1999) 5593.
- [27] (a) E. Ruiz, J. Cano, S. Alvarez, P. Alemany, *J. Am. Chem. Soc.* 120 (1998) 11122;
 (b) J. Ribas, A. Escuer, M. Monfort, R. Vicente, R. Cortes, L. Lezama, T. Rojo, *Coord. Chem. Rev.* 193–195 (1999) 1027.
- [28] M.E. Fisher, *Am. J. Phys.* 32 (1964) 343.
- [29] (a) K.S. Cole, R.H.J. Cole, *Chem. Phys.* 9 (1941) 341;
 (b) C.J.F. Boettcher, *Theory of Electric Polarization*, Elsevier, Amsterdam, 1952;
 (c) S.M. Aubin, Z. Sun, L. Pardi, J. Krzysteck, K. Folting, L.J. Brunel, A.L. Rheingold, G. Christou, D.N. Hendrickson, *Inorg. Chem.* 38 (1999) 5329.
- [30] (a) L. Bogani, R. Sessoli, M.G. Pini, A. Rettori, M.A. Novak, P. Rosa, M. Massi, M.E. Fedi, L. Giuntini, A. Caneschi, D. Gatteschi, *Phys. Rev. B* 72 (2005) 064406;
 (b) L. Bogani, A. Caneschi, M. Fedi, D. Gatteschi, M. Massi, M.A. Novak, M.G. Pini, A. Rettori, R. Sessoli, A. Vindigni, *Phys. Rev. Lett.* 92 (2004) 207204.
- [31] L.M. Toma, R. Lescouëzec, F. Lloret, M. Julve, J. Vaissermann, M. Verdaguer, *Chem. Commun.* (2003) 1850.
- [32] S. Gao, G. Su, S. Yi, B.Q. Ma, *Phys. Rev. B* 63 (2001) 054431.
- [33] (a) H. Miyasaka, R. Clerac, W. Wernsdorfer, L. Lecren, C. Bonhomme, K. Sugiura, M. Yamashita, *Angew. Chem., Int. Ed.* 43 (2004) 2801.
- [34] J. Yoo, E.K. Brechin, A. Yamaguchi, M. Nakano, J.C. Huffman, A.L. Maniero, L.C. Brunel, K. Awaga, H. Ishimoto, G. Christou, D.N. Hendrickson, *Inorg. Chem.* 39 (2000) 3615.
- [35] A. Caneschi, D. Gatteschi, N. Lalioti, R. Sessoli, L. Sorace, V. Tangoulis, A. Vindigni, *Chem. Eur. J.* 8 (2002) 286.
- [36] (a) L. Roland, V. Simonet, W. Wernsdorfer, L. Bogani, R. Sessoli, *J. Magn. Magn. Mater.* 272–276 (2004) 1079;
 (b) A. Lascialfari, E. Micotti, S. Aldrovandi, A. Caneschi, D. Gatteschi, *J. Appl. Phys.* 93 (2003) 8749;
 (c) E. Micotti, A. Lascialfari, A. Rigamonti, S. Aldrovandi, A. Caneschi, D. Gatteschi, L. Bogani, *J. Magn. Magn. Mater.* 272–276 (2004) 1087.
- [37] (a) N. Ishii, Y. Okamura, S. Chiba, T. Nogami, T. Ishida, *J. Am. Chem. Soc.* 130 (2008) 24;
 (b) R. Sessoli, *Angew. Chem., Int. Ed.* 47 (2008) 5508.
- [38] J. Seiden, *J. Phys. Lett.* 44 (1983) L947.
- [39] M. Drillon, E. Coronado, D. Beltran, R. Georges, *Chem. Phys.* 79 (1983) 449.
- [40] T. Kajiwara, R. Sensui, T. Noguchi, A. Kamiyama, T. Ito, *Inorg. Chim. Acta* 337 (2002) 299.
- [41] M.A.M. Abu-Youssef, A. Escuer, M.A.S. Goher, F.A. Mautner, G. Reiss, R. Vicente, *Angew. Chem., Int. Ed.* 39 (2000) 1624.
- [42] H. Kumagai, C.J. Kepert, M. Kurmoo, *Inorg. Chem.* 41 (2002) 3410.
- [43] C. Benelli, A. Caneschi, D. Gatteschi, R. Sessoli, *Adv. Mater.* 4 (1992) 504.
- [44] C. Benelli, A. Caneschi, D. Gatteschi, L. Pardi, P. Rey, *Inorg. Chem.* 29 (1990) 4223.
- [45] S. Mossin, H. Weihe, H.O. Sørensen, N. Lima, R. Sessoli, *Dalton Trans.* (2004) 632.
- [46] X.M. Zhang, Z.M. Hao, W.X. Zhang, X.M. Chen, *Angew. Chem., Int. Ed.* 46 (2007) 3456.
- [47] L.F. Jones, G. Rajaraman, J. Brockman, M. Murugesu, E.C. Sanudo, J. Raftery, S.J. Teat, W. Wernsdorfer, G. Christou, E.K. Brechin, D. Collison, *Chem. Eur. J.* 10 (2004) 5180.
- [48] F. Pan, Z.M. Wang, S. Gao, *Inorg. Chem.* 46 (2007) 10221.